Case Studies in Thermal Engineering 58 (2024) 104381

Contents lists available at ScienceDirect

Case Studies in Thermal Engineering

journal homepage: www.elsevier.com/locate/csite

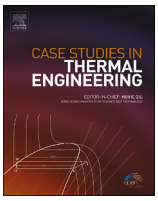

Optimal control of thermoregulation in the human dermal regions investigated through the stochastic integrated techniques

Iftikhar Ahmad [a], Syed Ibrar Hussain [b, c, *], Hira Ilyas [d], Muhammad Asif Zahoor Raja [e], Sana Afzal [a], Mariam Javed [a]

[a] Department of Mathematics, University of Gujrat, 50700, Pakistan
[b] Department of Mathematics and Computer Science, University of Palermo, Via Archirafi 34, 90123, Palermo, Italy
[c] Department of Mathematics, University of Houston, 77204, TX, USA
[d] Department of Physical Sciences, University of Chenab, Gujrat, Pakistan
[e] Future Technology Research Centre, National Yunlin University of Science and Technology, 123 University Road, Section 3, Douliou, Yunlin, 64002, Taiwan, ROC

ARTICLE INFO

Keywords:
Artificial neural networks (ANN)
Thermoregulation
Human dermal region (HDR)
Bioheat equation (BHE)
ANOVA

ABSTRACT

In this research, stochastic computing techniques based on artificial neural networks are applied to the proposed singular nonlinear differential equation to explain thermoregulation in the human dermal region problem to investigate and predict the effect of bioheat temperature on human skin at different atmospheric temperatures with different cases with considering the impact of both air convection thermal sensitivity and temperature, where sequential quadratic programming, interior point technique, and active set technique are included in the designed techniques. Moreover, thermal dynamics in the epidermal layer that is affected by both cooling and heating treatments, and the temperature profile across space and time have been examined. Numerical convergence analysis has been applied to endorse the nature of precision and convergence of the designed stochastic computing techniques. To preserve thermal balance, this leads to modifications in the human body's temperature regulation. The statistical analysis is provided comprehensively in the form of graphs and tables to further enhance the significance in terms of accuracy, efficiency, and convergence of the current study.

1. Introduction

The skin is the largest organ in the body that plays an essential part in thermoregulation, prevents excessive transpiration of water from the body, and provides defense against exterior chemical, physical, and biological threats. Each layer of the skin experiences bioheat transfer through conduction, which is brought on by the movement of vibrating atoms from high temperatures to the microscopic range, where they vibrate the originally stationary atoms as well. The imbalance in environmental temperature appears as a disorder of thermoregulation of the human system. Environmental temperatures shuffle their way via the dermal layer and tip to hyperthermia and hypothermia. Then finally advances to the body core and tissue necrosis to the body peripherals. The human body survives in different temperatures and conditions. The skin and core temperature regulation maintain the human body temperature [1–4]. Khanday and Saxena demonstrated various models to clarify the concept of thermoregulation in biological tissues. Thermal conductivity was invoked as a continuous function of temperatures. They contributed to the division of temperatures in boundaries of

* Corresponding author. Department of Mathematics and Computer Science, University of Palermo, Via Archirafi 34, 90123, Palermo, Italy.
E-mail addresses: dr.iftikhar@uog.edu.pk (I. Ahmad), syedibrar.hussain@unipa.it, syedhussain.ibrar@gmail.com (S.I. Hussain), hira@phs.uchenab.edu.pk (H. Ilyas), rajamaz@yuntech.edu.tw (M.A.Z. Raja), afzalsana04@gmail.com (S. Afzal), mariamjaved652@gmail.com (M. Javed).

https://doi.org/10.1016/j.csite.2024.104381
Received 25 January 2024; Received in revised form 29 March 2024; Accepted 9 April 2024
Available online 14 April 2024
2214-157X/© 2024 The Authors. Published by Elsevier Ltd. This is an open access article under the CC BY-NC-ND license (http://creativecommons.org/licenses/by-nc-nd/4.0/).

multi-layered skin and sub-dermal tissues. They introduced variational finite element methods about surrounding temperatures. They estimated the thermo-state phenomena of brain tissue and predicted the cold strain at various layers of the human head with the help of climate temperature [5–8].

The desired precise knowledge of thermal tolerances of human tissue and its cellular nature and physical changes caused by hyperthermia was not felt by the individual who not only supported their military staff and medical care but also for such development-effective weapons, nuclear bombs, and various other indiscriminate or explosive missiles, for pitching the spark to their development and use. As a cancer treatment method, Hyperthermia has a long history, about 3000 B.C. During the Second World War human history, due to heat has become a major cause of disability and death [9–14]. In 1947, Herrigues and Moriz formulated the model to determine the thermoregulation during various intensity surface and sub-surface exposures in the human dermal region [15]. Harry H. Penne's, determined in the upper skin extremity the cutaneous temperature effects regarding the presence of blood flow in the forearm and distribution of steady-state tissue temperature complexity, the temperature properties of warming agents in biological tissues, and analytic theory were applied to evaluate the various effects of heat [16]. In 1962, Perl. presented the theory of matter and heat distribution in human body tissues by utilizing the local clearance method to determine the rate of blood flow of tissue [17,18]. The collaboration of Richardson and Whitelaw Investigation evaluated the sudden effects and local changes of thermal load on human skin conductance, and these measurements were affected by blood flow rate. However, this approach proposed no idea for large skin areas for different rates of metabolism and changes that occur inside the skin itself [19]. U, FLESCH considered Thron's (1956) experimental findings, and his theoretical consideration acquired outcomes on the human head heat source distribution and what ensues if the environmental temperature changes, supposing a heat production level in a clear and compressive way [20]. Attempts had been made prior by Patterson (1976, 1978) for an experimental purpose of the temperature properties in the subcutaneous tissue's region [21]. Afterward in 1978, Saxena and Arya applied numerical and analytical methods to estimate temperature distribution in Subcutaneous tissues (SST), these mathematical methods did not pose effective outcomes [22–25].

Further in 1984, Saxena and Bindar applied the finite element method to estimate temperature distribution in steady-state human dermal regions, two imperative variables of blood flow rate and restraint heat generation of Metabolism [26]. Subsequently, in 1983, Diller and Layes analyzed thermoregulation by the condensed finite element method in the human dermal region [27]. In 1997 Yimin Xuan and W. Roetze presented a new bioheat model based on the principle of heat transfer porous media with consideration of temperature variation in the human body [28]. In 2000 Ng, Chua invoked Henriques' skin burns theory in combination with the two-dimensional model, Pennes equation of heat conduction for determining burn injury, and developed an axisymmetric two-dimensional model with a mesh-independent estimate and investigated human skin affected by the burning process [29]. The future efforts were made by Khandy and Saxena in 2009, who used the variational finite element method to assess the cold temperature. In 2010, Mamta Agrawal and Neeru Adlakha, and K. P. Pardasani endow two-dimensional temperature distribution in layers of diminished and elliptical-shaped extremities assisted by metabolic heat equation and variational method [30]. Gurung D B, Saxena V P & Adhikary P R considered only three layers of skin tissue and determined unsteady state one-dimensional temperature distribution in the human dermal region with quadratic function by utilizing the finite element method [31,32].

In 2012, D. B Garung utilized the finite element method to estimate a two-dimensional temperature distribution model at low environmental temperatures [33]. In 2012, Emmanuel Kengne, Ahmed Lakhssassi, and Rémi Vaillancourt assisted in temperature distributions in the dermal region by applying the Jacobi elliptic function and investigated the hypothermia situation in dermal subcutaneous tissues [34]. Afterward, in 2013, M. A Khanday conducted an endeavor on various dermal layers and SST. The authors have used multiple numerical techniques for analyzing the partial differential equation [35–38] that presents the biological, physical, chemical, and fluidic models in Refs. [39–41]. The bio heat model was earlier analyzed by Sur et al. by applying multiple numerical techniques [42–45]. Abbas et al. has used the multiple numerical techniques for analyzing the various kinds of differential equations, also analyzing the partial differential equations, especially by using the finite element methods [46–48]. Numerical techniques are used for analyzing the multiple kinds of biological models by the authors in Refs. [49–51]. Fahmy et al. has used the boundary element method in various studies to analyze the multiple biological models, including the bio heat models [52–55]. The basic objective of our current research is to develop a model to evaluate thermoregulation in the human dermal region by using the Stochastic technique. The innovative contributions of the designed techniques are as follows.

- The design techniques including sequential quadratic programming, interior point technique, and active set technique are applied to the proposed bio-heat singular nonlinear differential equation model to elaborate the effect of bioheat temperature on human skin.
- The atmospheric temperatures are varied to investigate the effect on thermoregulation in the human dermal region.
- The performance evaluation of the designed techniques is confirmed via multiple executions in terms of absolute errors.

The remaining research article structure is designed as; Mathematical Formulation of the Bioheat Model explained in section 2, in section 3 the designing and modeling of the techniques are illustrated, and the Numerical Handling of the Problem is provided in section 4**.** The conclusion is debated in the last section.

2. Mathematical Formulation of the bioheat model

The thermoregulation model can be defined as a boundary value problem. The domain survey depends on the dermal region and as a formulation of the bioheat equation.

$$p\frac{d^2\hat{T}}{d\hat{r}^2}+\frac{2p}{\hat{r}}\frac{d\hat{T}}{d\hat{r}}+\hat{Q}=0, \tag{2.1}$$

With boundary conditions

$$\lim_{\hat{r}\to 0}\frac{d\hat{T}}{d\hat{r}}=0, and -p\left(\frac{d\hat{T}}{d\hat{r}}\right)_{\hat{r}=\hat{R}}=E\left(\hat{T}_b-\hat{T}_a\right). \tag{2.2}$$

where $\hat{r}$ rendering the radial distance,$\widehat{R}$ is at the circumference center of the circle, E designates altering into vapors, the temperature distribution $\widehat{T}$ represents the first order partial derivative, $\widehat{T}_a$ the ambient temperature, $\widehat{T}_b$ the temperature distribution at the boundary of the body, $\widehat{Q}$ represents the production of unit volume, and "p" is the capacity of the human dermal region to conduct.

The presentation of temperature bioheat activity of the body has been supposed as the term $\widehat{k}\left(\widehat{T}\right)=K_0\left(\widehat{T}-\widehat{T}_H\right)^n$. To calculate the temperature distribution of the mathematical model of human dermal layers has been assumed pursuing the partial differential equation of bioheat equation as [56]:

$$\rho_b c_b\frac{\partial\hat{T}}{\partial t}=\nabla\left(\widehat{K}\left(\widehat{T}\right)\nabla.\hat{T}\right)+\widehat{K'}\left(\widehat{T}\right)\nabla.\hat{T}+\hat{Q}, \tag{2.3}$$

Where,

- ∇ is a rendering operator of $\widetilde{T}$, $\widehat{Q}=\hat{q}\left(37-\widehat{T}\right)$.
- K, ρ_b and c_b represent tissue's thermal conductivity, density, and heat. Equations (2.1) and (2.2) can be defined as;

$$k_0\frac{d^2\hat{T}}{d\hat{r}^2}+\left(\frac{2k_0}{\hat{r}}\right)\left(\frac{d\hat{T}}{d\hat{r}}\right)+\frac{nk_0}{\left(\hat{T}-\hat{T}_H\right)}\left(\frac{d\hat{T}}{d\hat{r}}\right)^2+\frac{\hat{q}\left(37-\hat{T}\right)}{\left(\hat{T}-\hat{T}_H\right)^2}=0, \tag{2.4}$$

With boundary equation

$$\left(\frac{d\hat{T}}{d\hat{r}}\right)_{\hat{r}=0}=0,\hat{T}\left(\hat{R}\right)=\hat{T}_H, \tag{2.5}$$

We consider the transformation.

$$u=\hat{T}-\hat{T}_H\ and\ \ t=\frac{\hat{r}}{\hat{R}},0<t<1 \tag{2.6}$$

Using equation (2.6) in equations (2.4) and (2.5) can be written as

$$k_0\frac{d^2u}{dt^2}+\left(\frac{2k_0}{t}\right)\left(\frac{du}{dt}\right)+\frac{nk_0}{u}\left(\frac{du}{dt}\right)^2+\frac{q\left(37-u-T_H\right)\hat{R}^2}{u^n}=0, \tag{2.7}$$

With boundary condition

$$\frac{du}{dt}(0)=0,u(1)=0.\quad 0<t<1 \tag{2.8}$$

For $n=1$ and $\alpha=\frac{q\hat{R}^2}{k_0}$,

$$\frac{d^2u}{dt^2}+\left(\frac{2}{t}\right)\left(\frac{du}{dt}\right)+\frac{1}{u}\left(\frac{du}{dt}\right)^2+\left(\frac{\left(37-u-T_H\right)}{u}\right)\alpha=0, \tag{2.9}$$

$$u'(0)=0,u(1)=0.\quad 0<t<1 \tag{2.10}$$

The structural figure of the above second-order differential equation (2.9) has been shown in Fig. 1(a).

3. Designing & modeling of the techniques

3.1. Modeling of bioheat equation

A model of an object is a representation of a proposed structure to assist estimation and calculation. The basic description of a framework using mathematical language and concepts, the scheme of evolving a mathematical model named mathematical model-

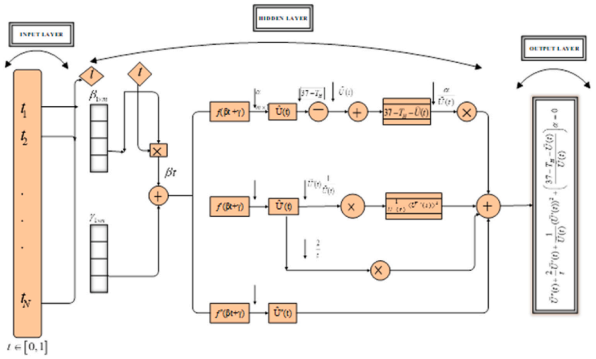

Fig. 1a. Structural diagram.

ing. ANN technique will be utilized to design the mathematical modeling of Bio heat equation. A neural network is named as a collection of neurons and computational neurons with the design associated with biological neurons [57–61].

$$\begin{aligned}
\widehat{u}(t) &= \sum_{m=1}^{N} \alpha_m f\left(\beta_m + \gamma_m\right), \\
\frac{d\widehat{u}(t)}{dt} &= \sum_{m=1}^{N} \alpha_m \frac{d}{dt}\left[f\left(\beta_m t + \gamma_m\right)\right], \\
\frac{d^2\widetilde{u}(t)}{dt^2} &= \sum_{m=1}^{N} \alpha_m \frac{d^2}{dt^2}\left[f\left(\beta_m t + \gamma_m\right)\right], \\
\frac{d^N\widehat{u}(t)}{dt^N} &= \sum_{m=1}^{N} \alpha_m \frac{d^N}{dt^N}\left[f\left(\beta_m t + \gamma_m\right)\right].
\end{aligned} \tag{3.1}$$

During the study, ANNMM of the bioheat equation utilizing feed-forward ANN is composed as continuous mapping for solution $\widetilde{u}(t)$ and its derivatives. In this research work, we consider the Artificial Neural Network (ANN) technique for nonlinear singular differential equations with boundary conditions. Artificial neural network (ANN) modeling is a function used for nonlinear singular differential equations with boundary conditions via continuous functions to estimate the approximate solution [62–67].

The mathematical modeling has utilized radial base f_{RB}, log-sigmoid f_{LS} functions and tan-sigmoid f_{TS} for indefinite covering of neural network as:

$$f_{RB}(t) = e^{-t^2}, \tag{3.2}$$

$$f_{LS}(t) = \frac{1}{1+e^{-t}}, \tag{3.3}$$

$$f_{TS}(t) = \frac{1}{1+e^{-2t^2}} - 1. \tag{3.4}$$

This research work, considers only radial-based activation function for the numerical treatment of the system.

$$f(t) = e^{-t^2}, \tag{3.5}$$

$$\widehat{u}(t) = \sum_{m=1}^{N} \alpha_m e^{-\left(\beta_m t+\gamma_m\right)^2}, \tag{3.6}$$

$$\frac{d\widehat{u}(t)}{dt} = \sum_{m=1}^{N} -e^{\left(\beta_m t+\gamma_m\right)^2} 2\alpha_m\beta_m\left(\beta_m t+\gamma_m\right)\left(\frac{\pi}{2}-\theta\right), \tag{3.7}$$

$$\frac{d^2\widehat{u}(t)}{dt^2} = \sum_{m=1}^{N} e^{-\left(\beta_m t+\gamma_m\right)^2} 2\alpha_m\beta_m^2\left(-1+2\left(\beta_m t+\gamma_m\right)^2\right). \tag{3.8}$$

Here α_m,β_m,γ_m are optimization weights.

3.2. Fitness function

The fitness function is defined as the sum of the mean square error in an unverified technique. Let us suppose the sum of two mean-square errors E_r. Let E_{r_1} and E_{r_2} are the mean square errors E_r, defined as

$$E_r = E_{r_1} + E_{r_2}, \tag{3.9}$$

Where E_{r_1} is fitness error function, related with second order on linear differential equation (2.9), can be written as

$$E_{r_1} = \frac{1}{M}\sum_{i=1}^{M}\left[k_0\frac{d^2\hat{u}_i}{dt^2} + \frac{2k_0}{t_i}\frac{d\hat{u}_i}{dt} + \frac{nk_0}{u_i}\left(\frac{d\hat{u}_i}{dt}\right)^2 + \frac{\alpha\left(37-\hat{u}_i-T_H\right)}{\hat{u}_i}\right]^2, \tag{3.10}$$

Additionally, E_{r_2} is an error fitness function that emerges from the boundary conditions.

$$E_{r_2} = 12\left[\left(\hat{u}_0-1\right)^2 + \left(\hat{u}_1-0\right)^2\right], \tag{3.11}$$

Where $N = \frac{1}{h}, \hat{u}_i = \hat{u}\left(\dot{t}_i\right), and\ \left(\dot{t}_i\right) = ih.$

3.3. Algorithm and flow chart of optimization technique

Firstly, utilize the necessities of the given problem by fixing the solvers. In this next step, set the numerical value of the scheme based on the random allocation and statements from the parameter setting scheme table. Now for the first two types of modeling, evaluate the fitness function of each population by using eq. (3.10) and eq. (3.11). Now procedure jumps for fitness function estimation. If it approaches the criteria, saves the results, and then terminates otherwise it will jump back again. The flow chart and the structural diagram of the proposed methodology are presented in Fig. 1(a and b).

4. Numerical Handling of the problem

In this section, we will discuss numerical conditions and estimate the outcomes through SQP, IPT, and AST techniques with different methodologies that have been utilized as follows in the given cases:

Case 1. Consider case, at $T_a = 0$, for p = 13, q = 0.000002 $\widehat{T}_H^2$, $\widetilde{T}_H = 33.03 + 0.14(\widehat{T}_a - 10)$, $k_0 = 0.00009\ \widehat{T}_H\left(37-\widehat{T}_H\right)^{-13}$, m = 10. Substituting all above values in equation (2.9) to get the following equation.

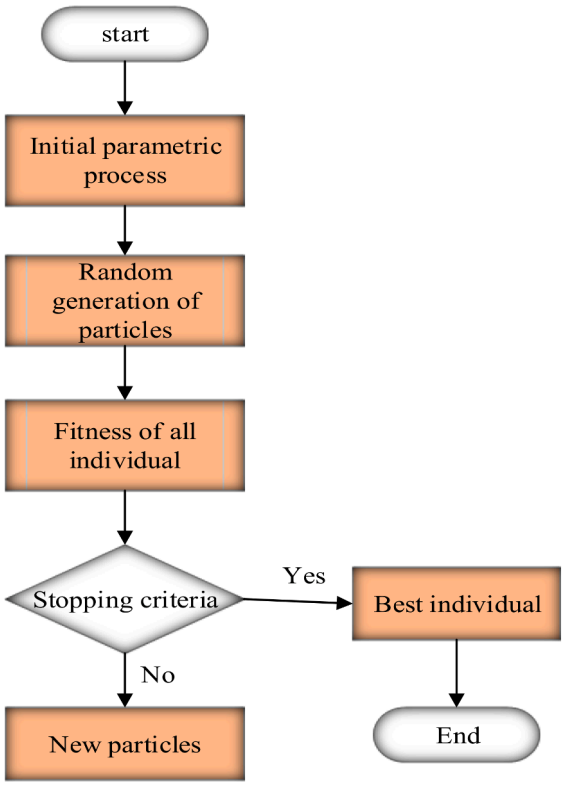

Fig. 1b. Flowchart of methodology for the proposed problem.

$$\frac{d^2}{dt^2}u(t)+\frac{2}{t}\frac{du}{dt}+\frac{1}{u}\left(\frac{d}{dt}u(t)\right)^2+\frac{(5.37-u)}{u}(0.1308)=0, \tag{4.1}$$

With boundary conditions

$$\frac{du}{dt}(0)=0, \tag{4.2}$$

$$u(1)=0. \tag{4.3}$$

The basic purpose of our study is to determine the solution of differential equations with proposed methodology. The fitness function for second order differential equation by equation (3.10) is given below.

$$E_{r_1}=\frac{1}{M}\sum_{i=1}^{M}\left[k_0\frac{d^2\hat{u}_i}{dt^2}+\frac{2k_0}{t_i}\frac{d\hat{u}_i}{dt}+\frac{nk_0}{u_i}\left(\frac{d\hat{u}_i}{dt}\right)^2+\frac{0.1308\left(37-\hat{u}_i-T_H\right)}{\hat{u}_i}\right]^2, \tag{4.4}$$

Where $M=30$,$h=0.1$, $t_i=ih$ and $\hat{u}_i=\hat{u}(t_i)$.

SQP, IPT and AST techniques determine the solution of equation (4.1) in accordance with (3.7) can be followed as a neuron. For $M=10$ and step size $h=0.1$ and weights functions are α, β, and γ respectively.

$$\hat{u}(t)=\frac{\alpha_1}{e^{(\beta_1 t+\gamma_1)^2}}+\frac{\alpha_2}{e^{(\beta_2 t+\gamma_2)^2}}+\frac{\alpha_3}{e^{(\beta_3 t+\gamma_3)^2}}+\ldots+\frac{\alpha_{10}}{e^{(\beta_{10} t+\gamma_{10})^2}}. \tag{4.5}$$

The optimal techniques present the proposed solution of equation (4.1) that can be composed of neurons. The techniques SQP, IPT, and AST estimate the numerical results by setting neurons N = 10, which are defined as terms of series solution $\hat{u}(t)$. Figure (2(a, b), 3) shows the training procedure for the optimization of the proposed methods SQP, IPT, and AST, taking as M = 10 with step size as h = 0.1 where the Tables (2–4) show the best numerical values of the weights that provides the close results to the reference solution from SQP, IPT and AST techniques. Additionally, these figures illustrate that the number of iterations increases as the function value approaches zero explains the activation function properly trained, and current point subfigures explain the range of the weight's values. The inputs for the numerical solution of equation (4.4) select variable values within 0 and 1, setting step size as h = 0.1. Table 5 compares the numerical values of the proposed methodologies SQP, IPT, and AST. Fig. 4 compares the nature of numerical results obtained from the designed techniques that explain as time increases the temperature decreases this implies both have inverse relations in nature. The IPT gives the best numerical values concluded from this figure, for more clarity the absolute error of IPT with SQP and AST is calculated and shown graphically in Fig. 5, tabulated in Table 6 which explains the accuracy and efficiency of the designed techniques. Figure (6-7) expresses the 2-dimensional plot for the numerical values having weights α, β and γ by neurons network over the optimization techniques SQP and IPT, also figure (7-8) shows the 3-dimensional plot for the numerical values having weights α, β, and γ. From eq. (4.6) to eq. (4.8) presenting the 2-dimensional and 3-dimensional graphs for the numerical values having weights α, β, and γ with 10 neurons. The weight's graphical and tabular representation describes that a weight may be positive or negative. These

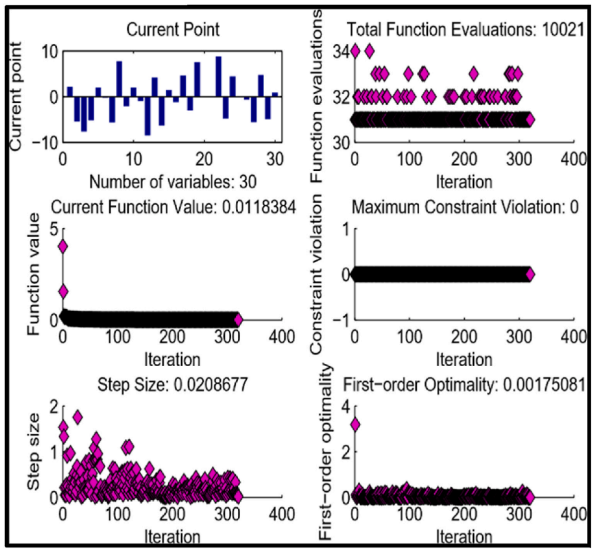

Fig. 2a. AST optimization fitness plots.

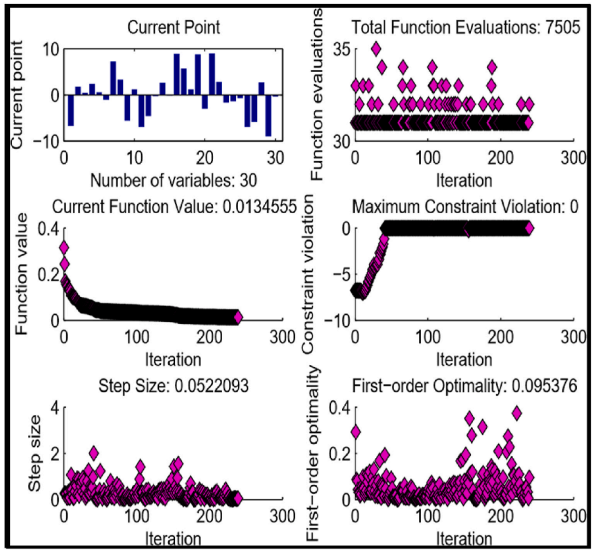

Fig. 2b. IPT optimization fitness plots.

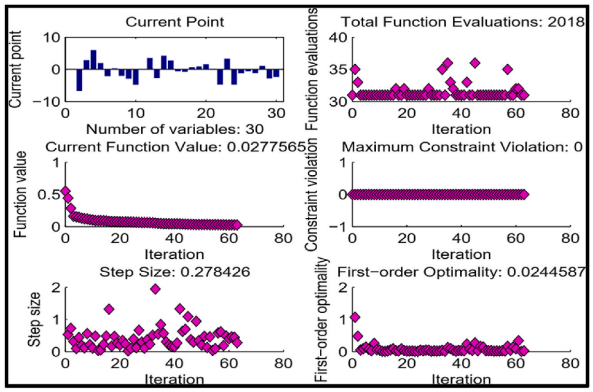

Fig. 3. SQP optimization fitness plots.

Table 1
Procedure's parameter setting.

Parameters	SQP	IPT	AST
Solver	FMINCON	FMINCON	FMINCON
Start Point	Random (1, 30)	Random (1, 30)	Random (1, 30)
Derivative	by Solver	Finite Central Difference	by Solver
Iteration	10,000	2000	10,000
X Patience	e−20	e−20	1e-20
Max Function study	10,000	1,000,000	15,000
Function Tolerance	e−20	e−20	1e-20
Constraints Tolerance	Default	Default	Default
Non-Linear Constraints	e−20	Nil	1e-20
Initial Weights, Hessian	Default	BFGS	Weights of AST
SQP Constrains, unboundedness Threshold	Default	Default	Nil

weights are put in equation (4.5) to get equation (4.6)-(4.8) which are the solutions of the proposed problem through designed techniques (see Fig. 9–11).

$$\widehat{u}_{[SQP]}(t) = \frac{(-0.02188)}{e^{(-0.05387t+0.098997)^2}} + \frac{(-6.73045)}{e^{(3.507983t+(-4.71929))^2}} + \frac{(2.871564)}{e^{(-2.68228t+3.337515)^2}} + \ldots + \frac{(-4.81367)}{e^{(1.559899t+(-2.37825))^2}}, \tag{4.6}$$

Table 2
The SQP Weights based on the Number of Neurons.

Solver	i	α_i	β_i	γ_i
SQP	1	−0.0218756	−0.0538692	0.098997
	2	−6.7304532	3.5079834	−4.7192943
	3	2.8715636	−2.6822757	3.3375148
	4	5.9883883	4.2730668	−4.7809386
	5	1.9536435	2.7962235	−1.1904801
	6	−2.1180752	−0.5781481	−0.5860977
	7	0.3538057	−0.7756455	−1.1555855
	8	−2.0087654	0.6433117	1.0798359
	9	−2.904809	0.9202398	−2.854459
	10	−4.8136736	1.5598989	−2.378247

Table 3
The IPT Weights based on the Number of Neurons.

Solver	i	α_i	β_i	γ_i
IPT	1	−2.165874	−3.191598	2.379201
	2	1.830870	1.528106	0.973129
	3	−1.433833	0.371903	0.1872533
	4	−1.086973	0.2691572	2.402688
	5	2.480237	−8.837678	8.220802
	6	−7.1288681	−7.2386734	7.3019036
	7	−5.256576	3.1911869	−3.5169145
	8	−2.9464109	0.5575582	−0.3329088
	9	8.5321772	−6.6117102	8.4968988
	10	0.5067896	−1.1455426	1.4835374

Table 4
The AST Weights based on the Number of Neurons.

Solver	i	α_i	β_i	γ_i
AST	1	2.68359	7.84390	−7.22291
	2	−2.90663	0.73727	−1.93769
	3	−7.95840	6.39565	−7.77017
	4	−5.86123	5.49601	−7.40871
	5	−3.66634	−0.00016	−0.69563
	6	2.91224	−9.00000	8.43098
	7	3.61447	0.30922	−0.59474
	8	−2.36062	−0.03135	2.19971
	9	8.97258	8.36467	−9.00000
	10	−8.39833	6.93559	−9.00000

Table 5
Comparison of numerical results of SQP, IPT and AST.

Parameter	Proposed Methods		
t	SQP	IPT	AST
0	0.282382789	0.108982905	0.349256759
0.1	0.281617368	0.108608662	0.347742159
0.2	0.278660455	0.107246684	0.343280727
0.3	0.273014121	0.104849238	0.336025453
0.4	0.264600291	0.101488901	0.325729580
0.5	0.253474061	0.097117147	0.311680276
0.6	0.239603852	0.091489190	0.293060791
0.7	0.222605300	0.084052427	0.269392644
0.8	0.201208850	0.073907838	0.238068057
0.9	0.172106237	0.060556873	0.196085596
1.0	0.127749685	0.037935764	0.124145560

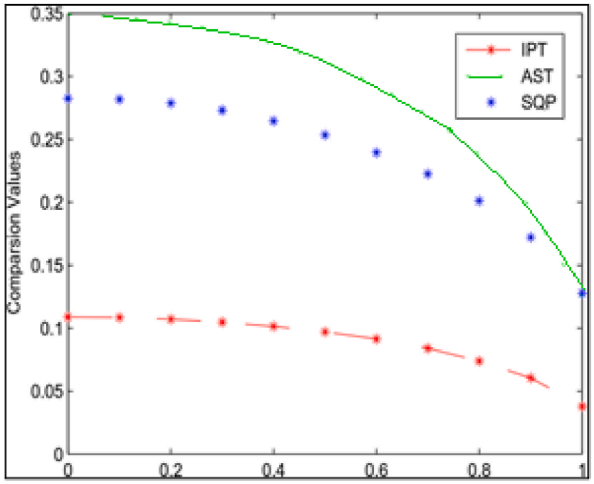

Fig. 4. Comparison of SQP, IPT and AST

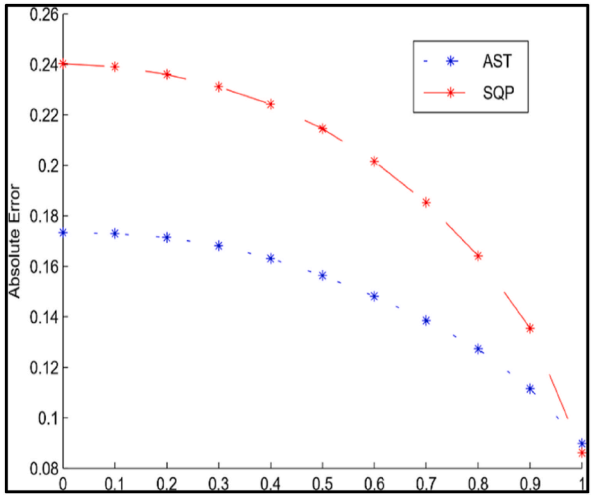

Fig. 5. Absolute error of SQP, IPT, and AST

Table 6
Comparison of absolute error of proposed methodology.

Relative Absolute Error ($\mid U_{ref} - U_{App} \mid$)			
Parameters	Proposed Methods		
t	IPT Ref. Sol	SQP	AST
0	0.108982905	0.173399884	0.240273854
0.1	0.108608662	0.173008706	0.239133497
0.2	0.107246684	0.171413771	0.236034043
0.3	0.104849238	0.168164883	0.231176215
0.4	0.101488901	0.163111390	0.224240679
0.5	0.097117147	0.156356914	0.214563129
0.6	0.09148919	0.148114662	0.201571600
0.7	0.084052427	0.138552872	0.185340216
0.8	0.073907838	0.127301011	0.164160219
0.9	0.060556873	0.111549364	0.135528723
1	0.037935764	0.089813921	0.086209799

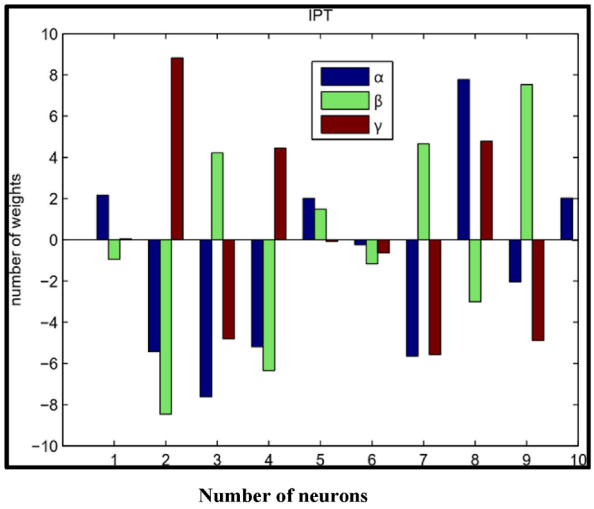

Fig. 6. 2-Dimensional weights of IPT.

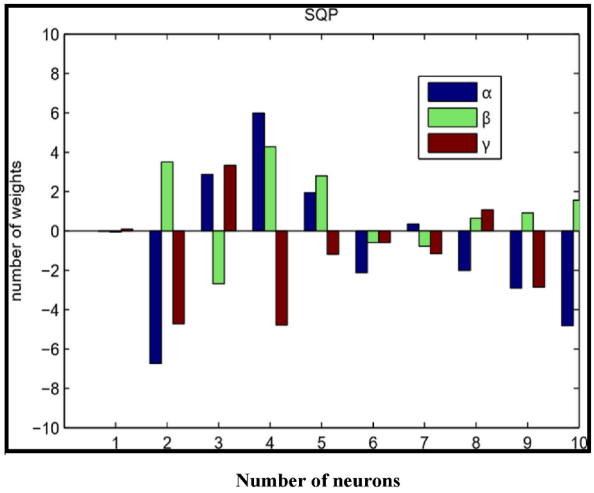

Fig. 7. 2-Dimensional weights of SQP.

$$\widehat{u}_{[IPT]}(t) = \frac{(-2.16587)}{e^{(-3.1916t+2.37920)^2}} + \frac{(1.83037)}{e^{(1.52810t+(0.97313))^2}} + \frac{(-1.43383)}{e^{(0.37190t+0.18725)^2}} + \ldots + \frac{(0.50679)}{e^{(-1.14554t+1.48353)^2}}, \tag{4.7}$$

$$\widehat{u}_{[AST]}(t) = \frac{(2.68359)}{e^{(7.84390t+(-7.22292))^2}} + \frac{(-2.68835)}{e^{(0.73727t+(-1.9377))^2}} + \frac{(-7.9584)}{e^{(6.39568t+(-7.77018))^2}} + \ldots + \frac{(-8.39833)}{e^{(6.93559t+(-9))2}}. \tag{4.8}$$

Case 2. Consider the case, at $T_a = 10$, for p = 13, q = 0.000002 $\widehat{T}_H^2$, $\widetilde{T}_H = 33.03 + 0.14(\widehat{T}_a - 10)$, $k_0 = 0.00009\ \widehat{T}_H \left(37 - \widehat{T}_H\right)^{-13}$ m = 10. Substituting all above values in equation (2.9) to get the following equation

$$\frac{d^2}{dt^2}u(t) + \frac{2}{t}\frac{du}{dt} + \frac{1}{u}\left(\frac{d}{dt}u(t)\right)^2 + \frac{(3.97-u)}{u}(0.1849) = 0, \tag{4.9}$$

With boundary condition

$$\frac{du}{dt}(0) = 0, \tag{4.10}$$

$$u(1) = 0. \tag{4.11}$$

The basic purpose of this study is to determine the solution of differential equations with proposed methodology. Fitness function for second order differential equation in accordance with (3.10) given as below.

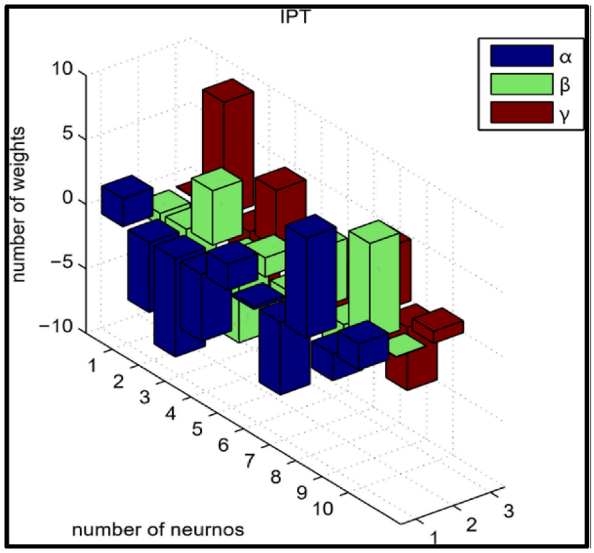

Fig. 8. 3-Dimensional weights of IPT

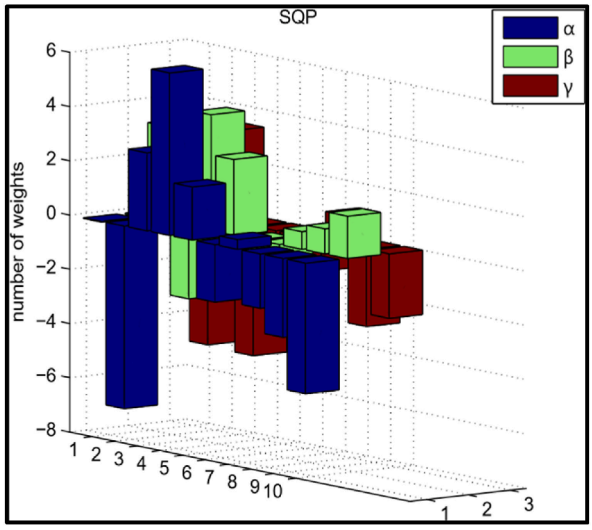

Fig. 9. 3-Dimensional weights of SQP.

$$E_{r_1} = \frac{1}{M}\sum_{i=1}^{M}\left[k_0\frac{d^2\hat{u}_i}{dt^2} + \frac{2k_0}{t_i}\frac{d\hat{u}_i}{dt} + \frac{nk_0}{u_i}\left(\frac{d\hat{u}_i}{dt}\right)^2 + \frac{0.1849\left(37-\hat{u}_i-T_H\right)}{\hat{u}_i}\right]^2, \tag{4.12}$$

Where $M = 30, h = 0.1$, $t_i = ih$ and $\hat{u}_i = \hat{u}(t_i)$.

$$\hat{u}(t) = \frac{\boldsymbol{\alpha_1}}{\boldsymbol{e}^{(\beta_1 t+\gamma_1)^2}} + \frac{\boldsymbol{\alpha_2}}{\boldsymbol{e}^{(\beta_2 t+\gamma_2)^2}} + \frac{\boldsymbol{\alpha_3}}{\boldsymbol{e}^{(\beta_3 t+\gamma_3)^2}} + \ldots + \frac{\boldsymbol{\alpha_{10}}}{\boldsymbol{e}^{(\beta_{10} t+\gamma_{10})^2}}, \tag{4.13}$$

$$\hat{u}_{[SQP]}(t) = \frac{(-4.73898)}{e^{(-0.04339t+(-8.36909))^2}} + \frac{(9)}{e^{(-7.20918t+(9))^2}} + \frac{(-4.26478)}{e^{(0.336845t+6.853676)^2}} + \ldots + \frac{(-0.0968136)}{e^{(7.8367813t+(-4.1728156))^2}}, \tag{4.14}$$

$$\hat{u}_{[IPT]}(t) = \frac{(-2.701974)}{e^{(-0.544762t+(-0.695625))^2}} + \frac{(0.282586)}{e^{(-0.916124t+0.190183)^2}} + \frac{(4.353871)}{e^{(-6.901859t+6.956632)^2}} + \ldots. + \frac{(8.1171462)}{e^{(-6.6935202t+8.3253128)^2}}, \tag{4.15}$$

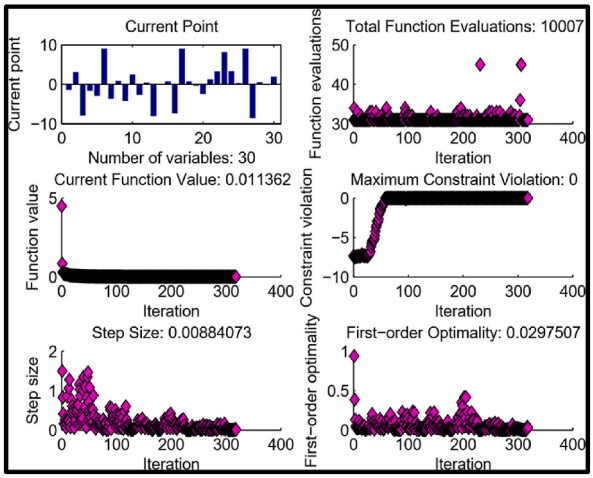

Fig. 10. Optimization fitness plots.

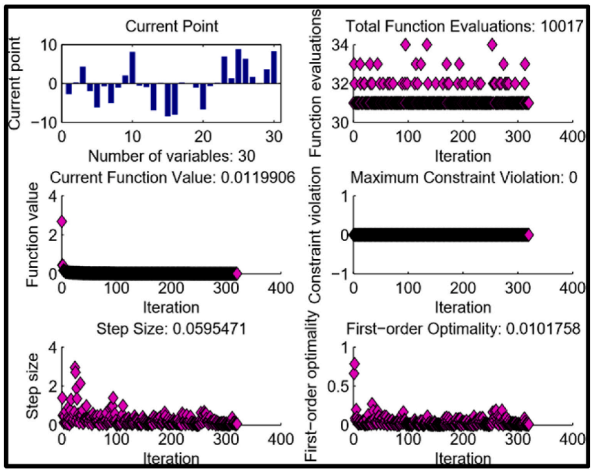

Fig. 11. IPT optimization fitness plots.

$$\widehat{u}_{[AST]}(t) = \frac{(-1.3893728)}{e^{(-2.6916434t+1.2937094)^2}} + \frac{(3.1351042)}{e^{(0.4219198t+(3.3023118))^2}} + \frac{(-7.9440465)}{e^{(-8.0606416t+8.1947170)^2}} + \ldots + \frac{(2.4990326)}{e^{(-2.4331333t+1.92250437)^2}}. \tag{4.16}$$

Optimal techniques present the proposed solution of equation (4.9) that can be composed of neurons (see Fig. 12). The techniques SQP, IPT, and AST estimate the numerical results by setting neurons N = 10, which are defined as terms of the series solution of $\hat{u}(t)$. The training procedure for the optimization of the proposed methods SQP, IPT, and AST corresponding to M = 10 with step size as h = 0.1 along with the training settings that are defined in Table 1 for the best optimization of the case explained in equation (4.9). Moreover, as the number of iterations increases the function value approaches zero which explains the activation function properly trained and current point subfigures explain the range of the weight's values. Tables (7–9) illustrate the best numerical weight values that provide close results to the reference solution through SQP, IPT, and AST techniques. Table 10 compares the numerical values obtained from the proposed methodologies SQP, IPT, and AST. Fig. 13 relates the nature of numerical results obtained from SQP, IPT, and AST with variable values between 0 and 1 as input and setting step size as h = 0.1, where this figure explains as time increases the temperature decreases this implies both have inverse relations in nature. Furthermore, from this figure, it has been seen that IPT gives the best numerical values. The absolute error of IPT with SQP and AST is shown in Fig. 14 and given in Table 11.

Figure 15 and 16 illustrates the 2-dimensional plot for the numerical values having weights α, β and γ by neurons network over the optimization techniques SQP, IPT, and AST, also figure 17 and 18 presents the 3-dimensional plot for the numerical values having weights α, β and γ. From eq. (4.14) to eq. (4.16) presenting the 2-dimensional and 3-dimensional graphs for the numerical values having weights α, β and γ with 10 neurons.

Case 3. Consider the case, at $T_a = 21$, for p = 13, q = 0.000002 $\widehat{T}_H^2$, $\widehat{T}_H = 33.03 + 0.14(\widehat{T}_a - 10)$, $k_0 = 0.00009\ \widehat{T}_H \left(37 - \widehat{T}_H\right)^{-13}$

Table 7
The SQP Weights based on the Number of Neurons.

Solver	i	α_i	β_i	γ_i
SQP	1	−4.738975	−0.043392	−8.369093
	2	9.0000000	−7.20917742	9.000000
	3	−4.264784	0.336845	6.853675
	4	0.868249101	0.687513327	6.414291386
	5	−3.852087	−0.708092	−5.941007
	6	−1.878569	9.000000	−8.538757
	7	−5.121022	−8.178188	8.459491
	8	0.505673	−8.117904	−6.860490
	9	1.619004	−5.337035	−7.598032
	10	−0.096813	7.836781	−4.172815

Table 8
The IPT Weights based on the Number of Neurons.

Solver	i	α_i	β_i	γ_i
IPT	1	−2.701974	−0.544762	−0.695625
	2	0.282586	−0.916124	0.190183
	3	4.353871	−6.901859	6.956632
	4	−1.957892	0.150348	1.392095
	5	−6.138193	−8.456369	8.820482
	6	−0.747294	−8.012749	6.334934
	7	−5.055056	0.247670	1.717538
	8	−1.077963	−0.079176	−0.145004
	9	2.048932	−1.074916	3.642906
	10	8.117146	−6.693520	8.325312

Table 9
The AST Weights based on the Number of Neurons.

Solver	i	α_i	β_i	γ_i
AST	1	−1.389372	−2.691643	1.293709
	2	−7.944046	−8.060641	8.194717
	3	3.135104	0.421919	3.302311
	4	−1.662032	−0.080898	3.338062
	5	−2.938966	0.766610	0.328500
	6	9.000000	−7.379876	9.000000
	7	−3.615284	9.000000	−8.580870
	8	0.883140	0.778215	0.559915
	9	−4.212019	−0.362640	−0.160036
	10	2.499032	−2.433133	1.922504

Table 10
Comparison of numerical results of SQP, IPT and AST.

Parameter	Proposed Methods		
t	SQP	IPT	AST
0	0.346357735	0.143227909	0.177820122
0.1	0.344940744	0.142538767	0.177004997
0.2	0.344940744	0.140705308	0.175053249
0.3	0.333208121	0.137810404	0.171442243
0.4	0.322100826	0.133587585	0.165850216
0.5	0.306937870	0.127593183	0.158278230
0.6	0.287306052	0.119603922	0.148619609
0.7	0.262302498	0.109604759	0.136461338
0.8	0.228837954	0.096304164	0.120224989
0.9	0.184544276	0.078467605	0.098432040
1	0.107599527	0.046562639	0.060576137

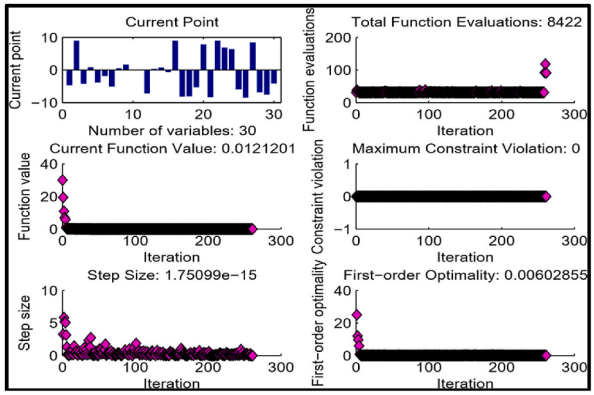

Fig. 12. SQP optimization fitness plots.

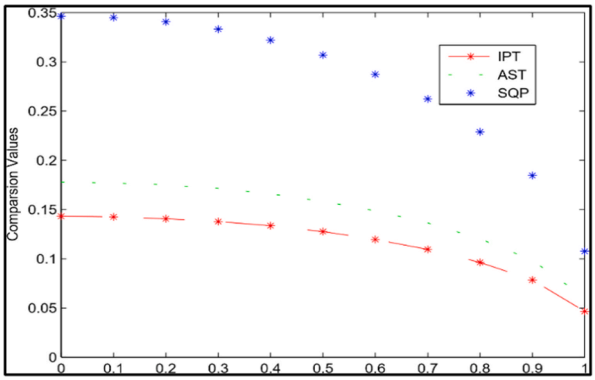

Fig. 13. Comparison of SQP, IPT and AST

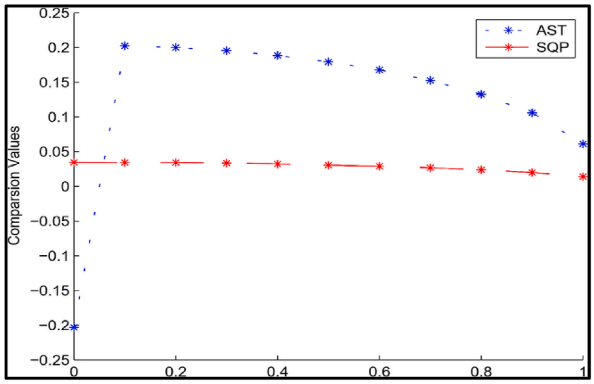

Fig. 14. Absolute error of SQP, IPT and AST

, m = 10. Substituting all the above values in equation (2.9) to get the following equation.

$$\frac{d^{213}}{dt^2}u(t)+\frac{2}{t}\frac{du}{dt}+\frac{1}{u}\left(\frac{d}{dt}u(t)\right)^2+\frac{(5.51-u)}{u}(0.1270)=0, \tag{4.17}$$

With boundary condition

$$\frac{du}{dt}(0)=0, \tag{4.18}$$

$$u(1)=0. \tag{4.19}$$

The basic purpose of our study is to determine the solution of differential equations with proposed methodology. Fitness function for second order differential equation in accordance with (3.10) given as below:

Table 11
Comparison of absolute error of proposed methodology.

Relative Absolute Error ($\mid U_{ref} - U_{App} \mid$)			
Parameters	Proposed Methods		
t	IPT Ref. Sol.	SQP	AST
0	0.143227909	0.203129826	0.034592213
0.1	0.14253877	0.202401978	0.03446623
0.2	0.140705308	0.199994023	0.03434794
0.3	0.137810404	0.188513241	0.033631839
0.4	0.133587585	0.188513241	0.032262631
0.5	0.127593183	0.179344687	0.030685046
0.6	0.119603922	0.16770213	0.029015687
0.7	0.109604759	0.152697739	0.02685658
0.8	0.096304164	0.132533791	0.023920825
0.9	0.078467605	0.106076672	0.019964436
1	0.046562639	0.061036888	0.014013498

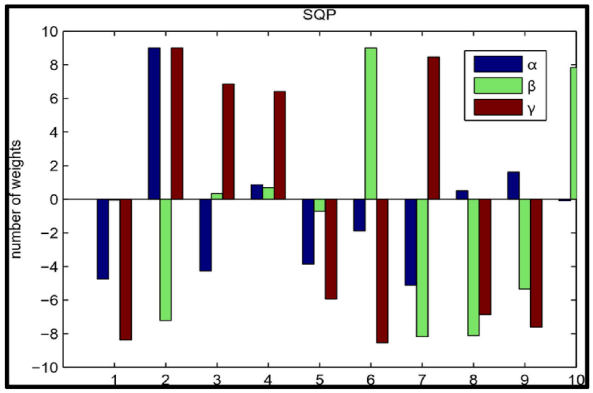

Fig. 15. 2-Dimensional weights of SQP.

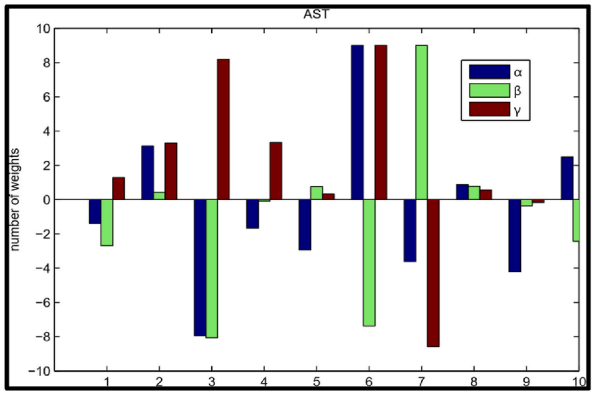

Fig. 16. 2-Dimensional weights of AST.

$$E_{r_1} = \frac{1}{M}\sum_{i=1}^{M}\left[k_0\frac{d^2\hat{u}_i}{dt^2} + \frac{2k_0}{t_i}\frac{d\hat{u}_i}{dt} + \frac{nk_0}{u_i}\left(\frac{d\hat{u}_i}{dt}\right)^2 + \frac{0.1849\left(37-\hat{u}_i-T_H\right)}{\hat{u}_i}\right]^2, \tag{4.20}$$

Where $M = 30, h = 0.1$, $t_i = ih$ and $\hat{u}_i = \hat{u}(t_i)$.

$$\hat{u}(t) = \frac{\alpha_1}{e^{(\beta_1 t+\gamma_1)^2}} + \frac{\alpha_2}{e^{(\beta_2 t+\gamma_2)^2}} + \frac{\alpha_3}{e^{(\beta_3 t+\gamma_3)^2}} + \ldots + \frac{\alpha_{10}}{e^{(\beta_{10} t+\gamma_{10})^2}} \tag{4.21}$$

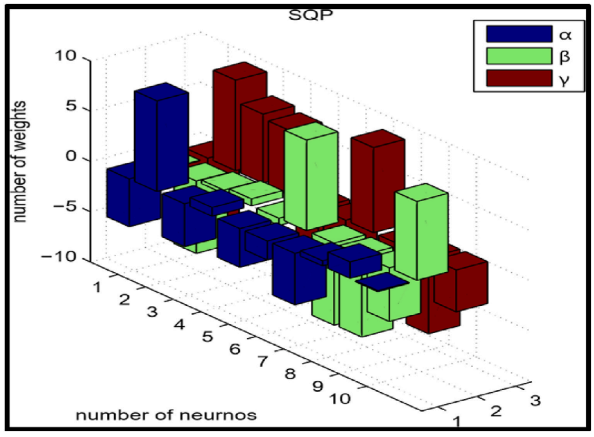

Fig. 17. 3-Dimensional weights of SQP.

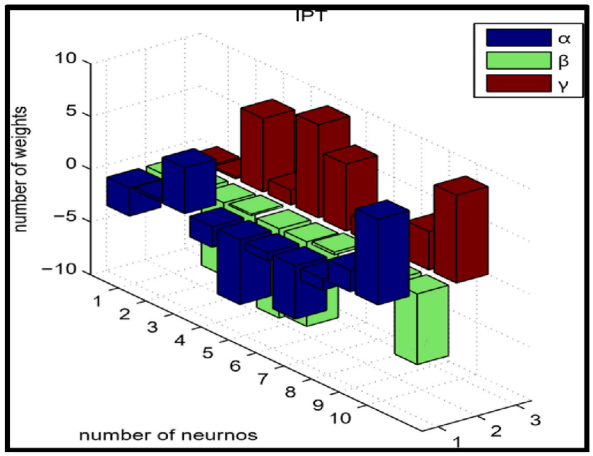

Fig. 18. 3-Dimensional weights of IPT.

$$\widehat{u}_{[SQP]}(t) = \frac{(2.2263233)}{e^{(-0.1666886t+(-0.2908640))^2}} + \frac{(-1.3141168)}{e^{(-1.6902360t+1.5187239)^2}} + \frac{(-0.1088466)}{e^{(-3.2096267t+0.2287175)^2}} + \ldots + \frac{(-2.9741339)}{e^{(0.8670136t+0.1049737)^2}}, \tag{4.22}$$

$$\widehat{u}_{[IPT]}(t) = \frac{(-0.2497133)}{e^{(-0.2142924t+2.2353841)^2}} + \frac{(3.3946270)}{e^{(1.9246459t+(-3.7926374))^2}} + \frac{(5.9893358)}{e^{(5.3495796t+-4.7940167)^2}} + \ldots\ldots\ldots\ldots + \frac{(1.3844345)}{e^{(-8.5285393t+7.9248469)^2}}, \tag{4.23}$$

$$\widehat{u}_{[AST]}(t) = \frac{(0.8208186)}{e^{(0.6682066t+0.7611549)^2}} + \frac{(-9)}{e^{(6.9213800t\pm8.7914004)^2}} + \frac{(3.2066868)}{e^{(-8.9897799t+8.6267777)^2}} + \ldots + \frac{(-0.0716043)}{e^{(-6.5879423t\pm1.2664913)^2}}. \tag{4.24}$$

Optimal techniques present the proposed solution of equation (4.17) that can be composed of neurons. The techniques SQP, IPT and AST estimate the numerical results by setting neurons N = 10, are defined as terms of series solution $\widetilde{u}(t)$. Figure 19 and 20 shows the training state of equation (4.17) assisted by optimization methods SQP, IPT and AST, taking as M = 10 with step size as h = 0.1. These figures explain the training of the proposed techniques at each iteration along the current points value, where the Tables (12–14) show the best numerical values of the trained weights through SQP, IPT, and AST for getting better outputs of the proposed problem. The inputs for the numerical solution of equation (4.20) select variable values between 0 and 1, setting step size as h = 0.1. Table 15 compares the numerical values of the proposed methodologies SQP, IPT, and AST. Fig. 21 illustrates the nature of numerical results obtained from SQP, IPT, and AST, additionally, the temperature decreases corresponding to the time passage. Moreover, in this figure, it has been seen that IPT gives the best numerical values. The absolute error of IPT with SQP and AST is shown in Fig. 22 and given in Table 16 which explains the accuracy and efficiency of the technique.

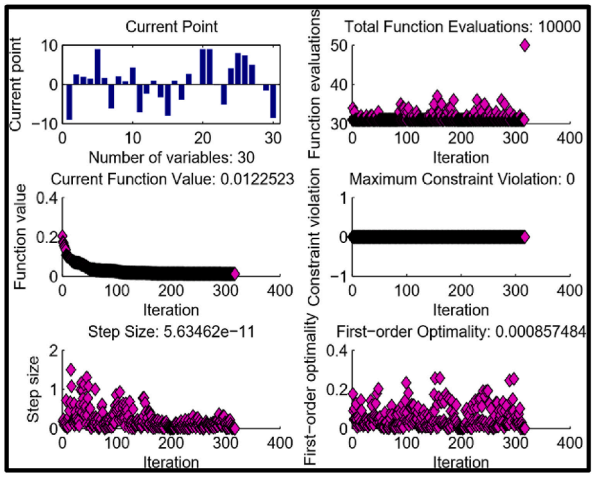

Fig. 19. SQP optimization fitness plots.

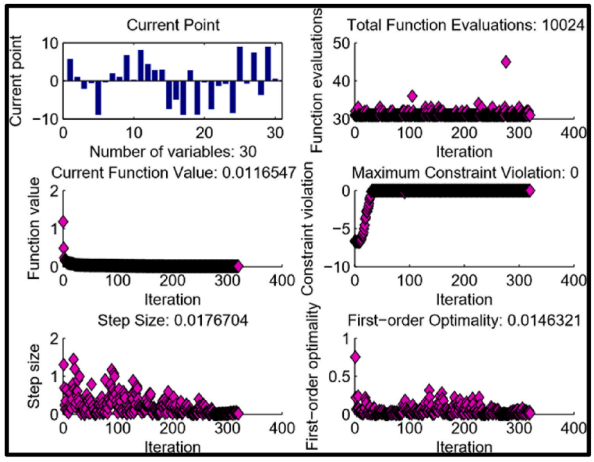

Fig. 20. AST optimization fitness plots.

Table 12
The SQP Weights based on the Number of Neurons.

solver	i	α_i	β_i	γ_i
SQP	1	2.226323309	−0.166688627	−0.290864039
	2	−1.314116888	−1.69023603	1.518723935
	3	−0.10884664	−3.209626748	0.228717568
	4	3.279619514	−0.960095292	−4.765585426
	5	0.563806859	−0.51720191	−1.540856242
	6	−0.994103939	−3.442424623	−1.91725382
	7	0.239462676	−0.194752596	−1.910649078
	8	−1.452061302	−2.397128559	1.961351405
	9	3.694807074	−1.972687197	2.896204728
	10	−2.97413395	0.867013605	0.104973723

Figure 23–25 shows the 2-dimensional plot for the numerical values having weights α, β and γ by neuron networks over the optimization techniques SQP, IPT, and AST. Also figure 26 and 27 expresses the 3-dimensional plot for the numerical values having weights α, β and γ. From eq. (4.22) to eq. (4.24) presenting the 2-dimensional and 3-dimensional graphs for the numerical values having weights α, β, and γ with 10 neurons.

Case 4. Consider case as, at $T_a = 21$, for p = 13, q = 0.000002 $\widehat{T}_H^2$, $\widetilde{T}_H = 33.03 + 0.14(\widehat{T}_a - 10)$, $k_0 = 0.00009\ \widehat{T}_H \left(37 - \widehat{T}_H\right)^{-13}$, m = 10. Substituting all the above values in equation (2.9) to get the following equation.

Table 13
The IPT Weights based on the Number of Neurons.

solver	i	α_i	β_i	γ_i
IPT	1	−0.249713319	−0.21429247	2.235384184
	2	3.394627078	1.924645913	−3.792637492
	3	5.989335857	5.349579610	−4.794016700
	4	−3.412365789	−8.253330002	8.534879532
	5	−7.269393661	4.687331524	−4.321449425
	6	−8.149653240	6.621714103	−8.470330102
	7	2.988842258	0.214578488	−0.016762767
	8	5.318404563	1.525012705	−3.660092960
	9	1.830027229	−0.717848543	0.388776909
	10	1.384434508	−8.528539306	7.924846984

Table 14
The AST Weights based on the Number of Neurons.

solver	i	α_i	β_i	γ_i
AST	1	0.8208186	0.668206694	0.761154922
	2	−9.0000000	6.921380015	−8.791400401
	3	3.206686845	−8.98977996	8.626777795
	4	−3.446659915	7.733086651	−7.221319085
	5	3.102928344	8.122982404	−7.26069323
	6	7.024004305	−7.062029553	9.0000000
	7	−1.596486513	1.22993299	−6.124286894
	8	−8.961604436	−8.634621992	9.0000000
	9	−2.370624968	0.312910285	0.235773289
	10	−0.071604388	−6.587942372	−1.266491379

Table 15
Comparison of numerical results of SQP, IPT and AST.

Parameter	Proposed Methods		
t	SQP	IPT	AST
0	0.38293235	0.447268166	0.480180346
0.1	0.381460323	0.445559244	0.478427102
0.2	0.377623537	0.440202159	0.473294405
0.3	0.370896957	0.43059224	0.464060363
0.4	0.360850818	0.416211499	0.450101495
0.5	0.346945189	0.396509566	0.430609822
0.6	0.328442328	0.370939878	0.404665108
0.7	0.304385105	0.338362031	0.371025683
0.8	0.272398372	0.295195788	0.326080672
0.9	0.229838846	0.238474175	0.266622407
1	0.163563922	0.141999694	0.166375662

$$\frac{d^2}{dt^2}u(t)+\frac{2}{t}\frac{du}{dt}+\frac{1}{u}\left(\frac{d}{dt}u(t)\right)^2+\frac{(1.87-u)}{u}(0.4175)=0, \tag{4.25}$$

With boundary condition

$$\frac{du}{dt}(0)=0, \tag{4.26}$$

$$u(1)=0. \tag{4.27}$$

The basic purpose of our study is to determine the solution of differential equations with proposed methodology. Fitness function for second order differential equation in accordance with (3.10) given as below.

$$E_{r_1}=\frac{1}{M}\sum_{i=1}^{M}\left[k_0\frac{d^2\hat{u}_i}{dt^2}+\frac{2k_0}{t_i}\frac{d\hat{u}_i}{dt}+\frac{nk_0}{u_i}\left(\frac{d\hat{u}_i}{dt}\right)^2+\frac{0.4175\left(37-\hat{u}_i-T_H\right)}{\hat{u}_i}\right]^2, \tag{4.28}$$

Where $M=30$,$h=0.1$, $t_i=ih$ and $\hat{u}_i=\hat{u}(t_i)$.

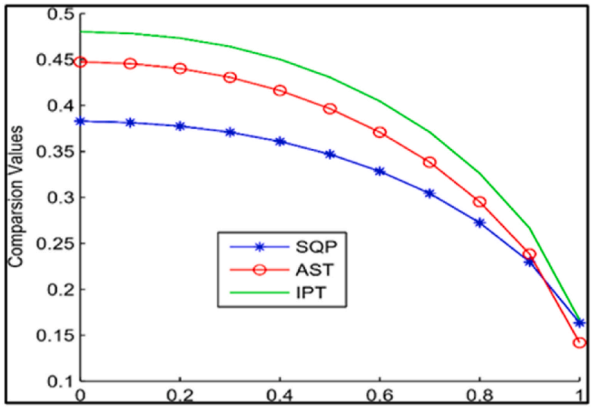

Fig. 21. Comparison of SQP, IPT and AST

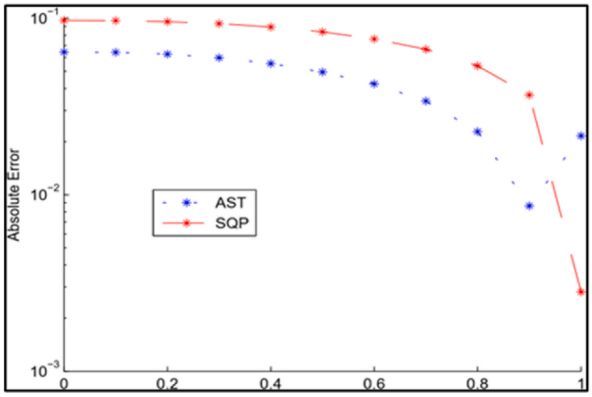

Fig. 22. Absolute error of SQP, IPT, and AST

Table 16
Comparison of absolute error of proposed methodology.

Relative Absolute Error ($\mid U_{ref} - U_{App} \mid$)			
Parameters	Proposed Methods		
t	IPT Ref. Sol.	SQP	AST
0	0.064335816	0.38293235	0.097247996
0.1	0.064098921	0.381460323	0.096966779
0.2	0.062578622	0.377623537	0.095670868
0.3	0.059695283	0.370896957	0.093163406
0.4	0.055360682	0.360850818	0.089250677
0.5	0.049564377	0.346945189	0.083664634
0.6	0.042497550	0.328442328	0.076222780
0.7	0.033976927	0.304385105	0.066640579
0.8	0.022797416	0.272398372	0.05368230
0.9	0.008635329	0.229838846	0.03678356
1	0.021564227	0.163563922	0.002811741

SQP, AST and IPT techniques determine the solution of equation (4.25) in accordance with (3.10) can be followed as neuron. For M = 10 and step size h = 0.1 and Weights function are α, β, γ respectively.

$$\widehat{u}(t) = \frac{\alpha_1}{e^{(\beta_1 t+\gamma_1)^2}} + \frac{\alpha_2}{e^{(\beta_2 t+\gamma_2)^2}} + \frac{\alpha_3}{e^{(\beta_3 t+\gamma_3)^2}} + \ldots + \frac{\alpha_{10}}{e^{(\beta_{10} t+\gamma_{10})^2}}, \tag{4.29}$$

$$\widehat{u}_{[SQP]}(t) = \frac{(0.6076398)}{e^{(2.2458361t+2.1439176)^2}} + \frac{(-6.9646671)}{e^{(-2.4986749t+0.2753588)^2}} + \frac{(5.6915422)}{e^{(-0.5031249t\pm3.1094396)^2}} + \ldots + \frac{(6.1704013)}{e^{(8.5175060t+(-9))^2}}, \tag{4.30}$$

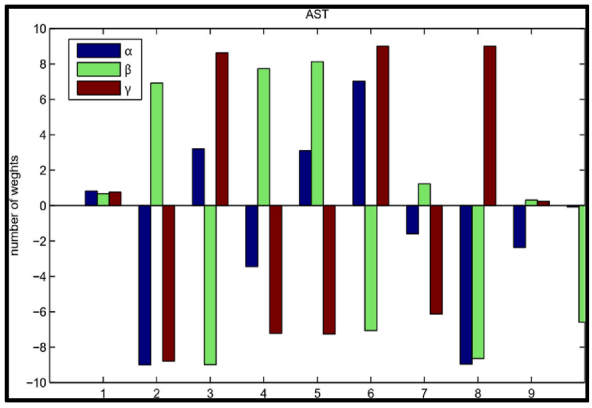

Fig. 23. 2-Dimensional weights of AST.

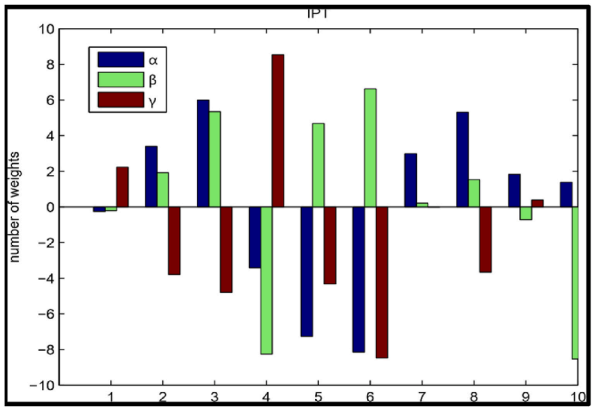

Fig. 24. 2-Dimensional weights of IPT.

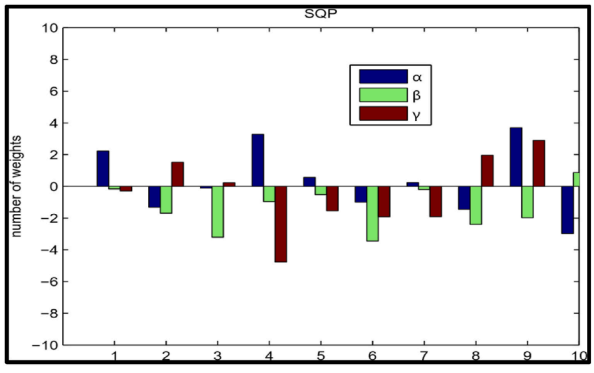

Fig. 25. 2-Dimensional weights of SQP.

$$\widehat{u}_{[IPT]}(\mathrm{t}) = \frac{(2.6748710)}{\mathrm{e}^{(-6.4389429\mathrm{t}+4.2818019)^2}} + \frac{(6.4854972)}{\mathrm{e}^{(-0.317767\mathrm{t}+(-1.841106))^2}} + \frac{(-3.4981012)}{\mathrm{e}^{(-2.2634920\mathrm{t}+-2.2832106)^2}} + \ldots\ldots + \frac{(-3.6759656)}{\mathrm{e}^{(8.5987303\mathrm{t}+-7.9395152)^2}}, \tag{4.31}$$

$$\widehat{u}_{[AST]}(t) = \frac{(\text{-}5.706521)}{e^{(0.461331\mathrm{t}+(\text{-}0.2193036))^2}} + \frac{(1.4990212)}{e^{(\text{-}0.8214061\mathrm{t}+(\text{-}0.9768137))^2}} + \frac{(\text{-}1.1323074)}{e^{(\text{-}0.4778924\mathrm{t}+(\text{-}1.7146891))^2}} + \ldots + \frac{(0.6627838)}{e^{(\text{-}0.2017040\mathrm{t}+(\text{-}1.2352638))^2}}. \tag{4.32}$$

Optimal techniques present the proposed solution of equation (4.25) that can be composed of neurons. The techniques SQP, AST, and IPT estimate the numerical results by setting neurons N = 10, are defined as terms of series solution $\tilde{u}(t)$. Figure 28–30 shows the

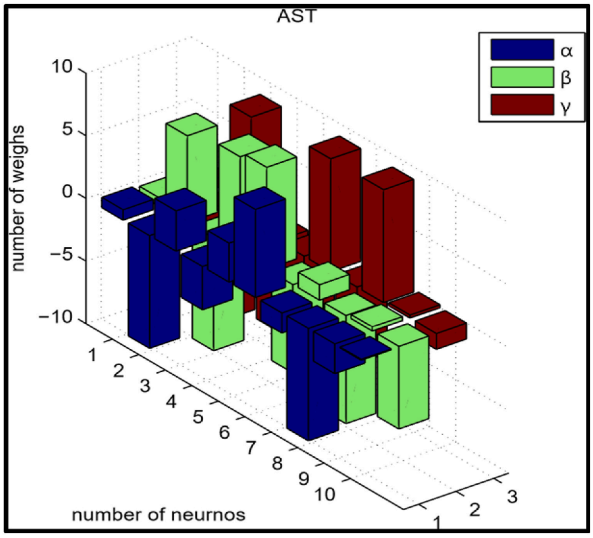

Fig. 26. 3-Dimensional weights of AST.

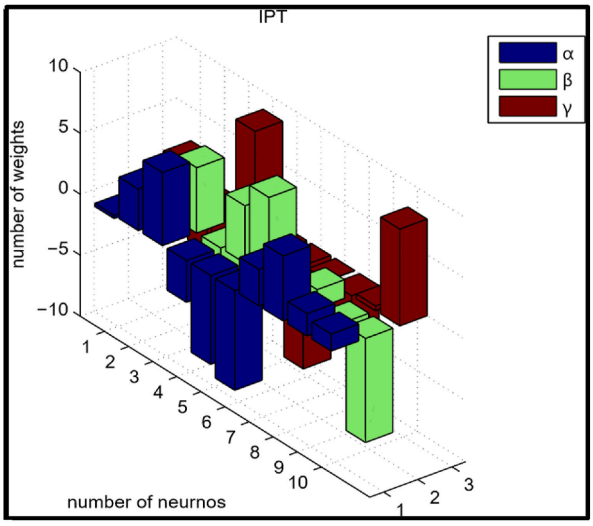

Fig. 27. 3-Dimensional weights of IPT.

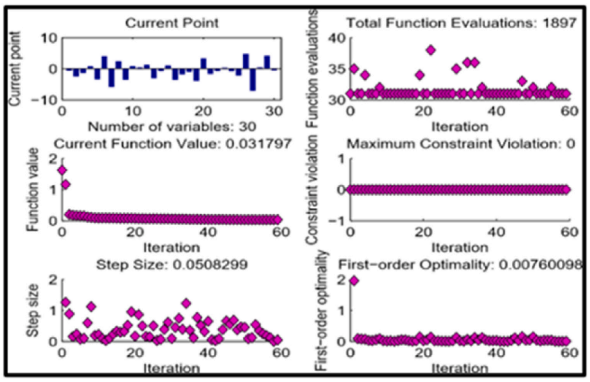

Fig. 28. SQP optimization fitness plots.

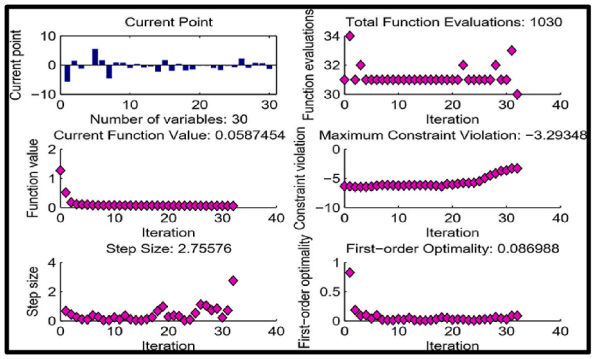

Fig. 29. AST optimization fitness plots.

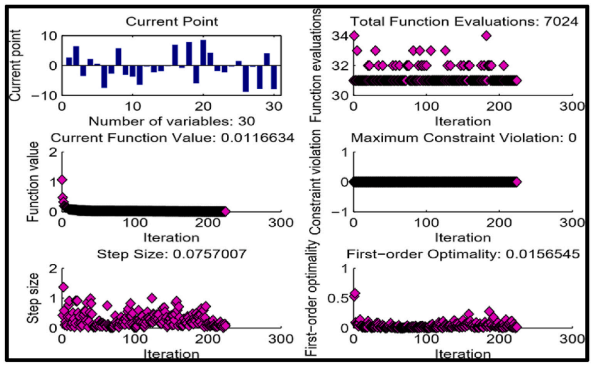

Fig. 30. IPT optimization fitness plots.

optimization training of equation (4.28) assisted by optimization techniques SQP, AST, and IPT**,** taking as M = 10 with step size as h = 0.1 which exploited the training procedure corresponding to the number of iterations and current points for the trained weights and the Tables (17–19) illustrate the weights that provides the best numerical results from SQP, AST and IPT. The inputs for numerical solution of equation (4.28) selects variable values within 0 and 1, setting step size as h = 0.1. The numerical values of the proposed methodologies SQP, AST, and IPT are tabulated in Table 20. Fig. 31 represents the nature of numerical results obtained from SQP, AST, and IPT that explain the effect of temperature related to time. From this figure, it has been seen that IPT gives the best numerical values. The absolute error of IPT with SQP and AST is shown in Fig. 32 and given in Table 21.

Figure 33 and 34 presents the 2-dimensional plot for the numerical values having weights α, β and γ in accordance with neurons network over the optimization techniques SQP, AST, and IPT. Also figure 35 and 36 shows the 3-dimensional plot for the numerical values having weights α, β and γ. From eq. (4.30) to eq. (4.32) presenting the 2-dimensional and 3-dimensional graphs for the numerical values having weights α, β and γ with 10 neurons. The weights graphical and tabular representation describes that a weight may be positive or negative.

Table 17
The SQP Weights based on the Number of Neurons.

Solver	i	α_i	β_i	γ_i
SQP	1	0.607639816	2.245836138	2.143917621
	2	−6.964667112	−2.498674924	0.275358803
	3	5.691542251	−0.503124985	−3.109439658
	4	9.000000000	−7.388437256	9.000000000
	5	−7.843471794	1.701476415	−0.705035062
	6	4.465206312	−1.198987133	0.453912615
	7	−4.263152431	7.698368215	−7.801227159
	8	2.070884090	−0.705791849	−0.854761737
	9	−6.183952347	−4.068757303	4.550785266
	10	6.170401329	8.517506025	−9.000000000

Table 18
The value of IPT of weights according to number of neurons.

Solver	i	α_i	β_i	γ_i
IPT	1	2.674871020	−6.438942958	4.28180199
	2	6.485497283	−0.317767416	−1.841106391
	3	−3.498101290	−2.263492086	−2.283210601
	4	2.140354357	−1.864909320	−0.316259635
	5	0.623866969	−0.223147627	1.488583274
	6	−7.475874865	7.005575902	−8.787887711
	7	−2.677109929	−0.800155288	−0.369566435
	8	5.806712731	7.88257660	−7.746760105
	9	−3.098097113	−5.943622387	4.127568531
	10	−3.675965635	8.598730391	−7.939515274

Table 19
The value of AST of weights according to number of neurons.

Solver	i	α_i	β_i	γ_i
AST	1	−5.706521526	0.461331141	−0.219303623
	2	1.499021215	−0.821406125	−0.976813717
	3	−1.132307413	−0.477892428	−1.714689106
	4	−0.17788710	−2.26304750	−0.25279370
	5	5.549892247	1.659262646	−0.779044275
	6	1.632663356	−1.897140202	2.257635973
	7	−4.573791107	0.495663904	−0.945345094
	8	0.856024900	−1.823967300	0.752877300
	9	0.799743570	−1.523394081	0.662783899
	10	−0.958381878	−0.201704079	−1.235263877

Table 20
Comparison of numerical results of SQP, AST and IPT.

Parameter	Proposed Methods		
t	SQP	IPT	AST
0	0.463991025	0.462081176	0.468045022
0.1	0.462055703	0.459716833	0.466255963
0.2	0.457843829	0.456129161	0.460843284
0.3	0.450435306	0.450473331	0.451102299
0.4	0.438971411	0.441643611	0.436535980
0.5	0.422607118	0.428320138	0.416924402
0.6	0.400328416	0.409117648	0.391705582
0.7	0.370583350	0.382268686	0.358820518
0.8	0.330916246	0.344865629	0.314880287
0.9	0.278104063	0.294217993	0.257471925
1	0.194934366	0.218169278	0.162770557

5. Conclusion and future recommendations

The behavior of the temperature distribution in the skin's multiple layers according to generalized boundary conditions has been investigated in this paper through computational scholastic numerical techniques including sequential quadratic programming (SQP), interior point technique (IPT), and active set technique (AST) that are used to optimize the solution that is close to the reference solution for deep understanding of the thermal dynamics in the epidermal layer that is affected by both cooling and heating treatments. The fitness function based on the radial function is considered to evaluate the fitness of the designed techniques by suitable optim-tool settings, it is concluded that the fitness values decrease as the iterations increase along with the current point which explains the range of the optimal weights from the figures of optimization fitness plot**s** SQP, AST, and IPT techniques. The statistical analysis tabulated in tables and graphically represented for all designed techniques demonstrates that IPT gives adequate results as compared to AST and SQP, furthermore, IPT converges to the reference solution faster as compared to AST and SQP, AST gives more reliable results as compared to SQP. The numerical results illustrated that temperature changes correspond to time which explains the dynamics of the thermal distribution in the multiple layers of the epidermis and are analyzed mathematically for boundary limit conditions over both cooling and heating processes, via the bioheat equation model.

Afterward, future work can be designed on dependent techniques in accordance with neural networks to search out, study, and relate to numerical results.

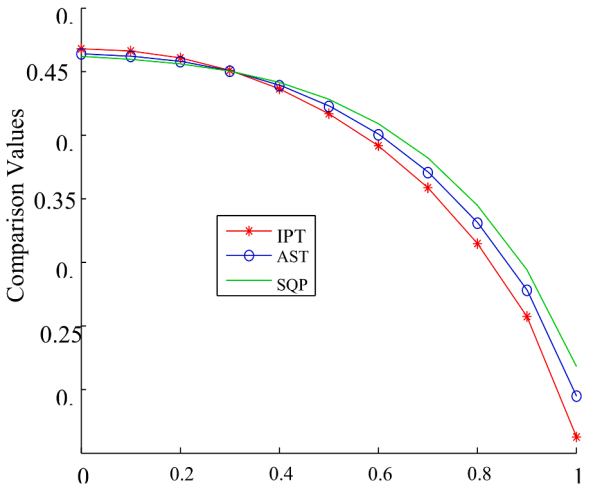

Fig. 31. Comparison of SQP, IPT and AST

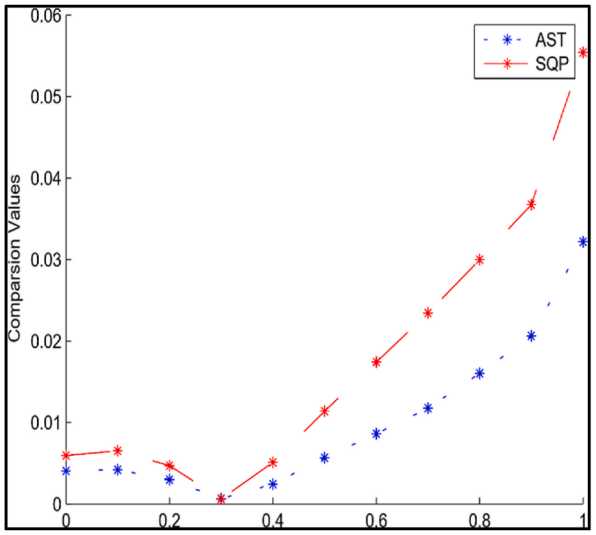

Fig. 32. Absolute error of SQP, IPT, AST

Table 21
Comparison of Absolute Error of Results of AST, SQP with Reference solution IPT.

Relative Absolute Error ($\mid U_{ref} - U_{App} \mid$)			
Parameters	Proposed Methods		
t	IPT Ref. Sol.	SQP	AST
0	0.468045022	0.004053997	0.005963847
0.1	0.466255963	0.004200259	0.006539129
0.2	0.460843284	0.002999455	0.004714122
0.3	0.451102299	0.000666993	0.000628967
0.4	0.43653598	0.002435431	0.005107632
0.5	0.416924402	0.005682716	0.011395736
0.6	0.391705582	0.008622834	0.017412066
0.7	0.358820518	0.011762832	0.023448168
0.8	0.314880287	0.016035960	0.029985343
0.9	0.257471925	0.020632138	0.036746068
1	0.162770557	0.032163809	0.055398721

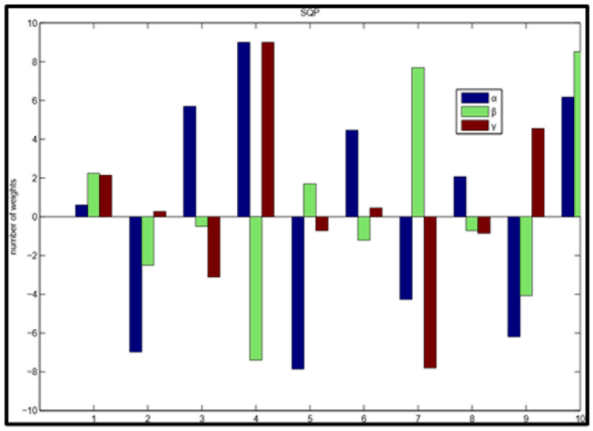

Fig. 33. 2-Dimensional weights of IPT.

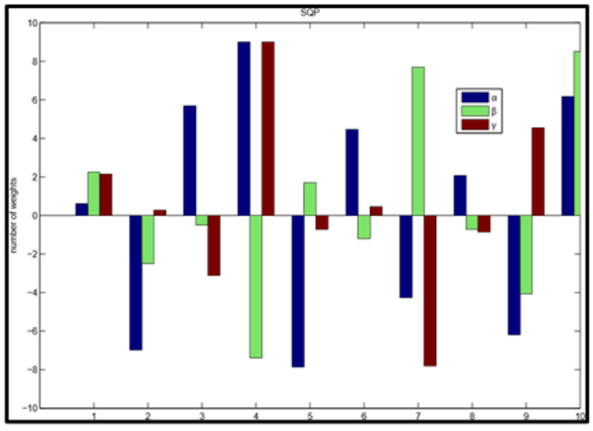

Fig. 34. 2-Dimensional weights of SQP.

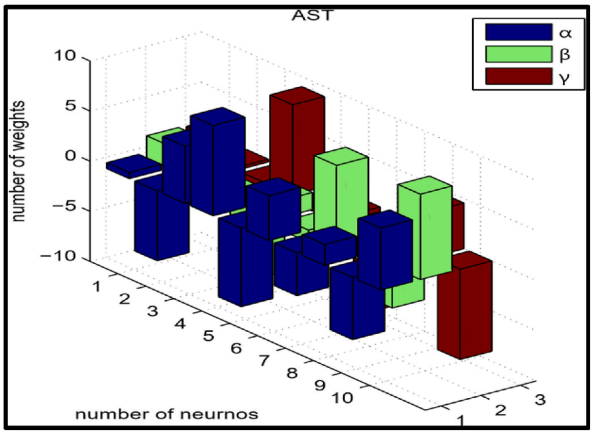

Fig. 35. 3-Dimensional weights of AST.

Ethical statements:

All the authors declare that:

- All authors have been personally and actively involved in substantial work leading to the paper and take public responsibility for its content.
- This material is the author's original work, which has not been previously published elsewhere.
- The paper is not currently being considered for publication elsewhere.

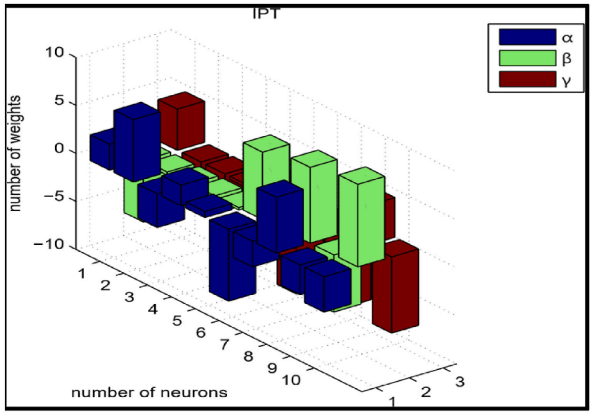

Fig. 36. 3-Dimensional weights of IPT.

- The paper reflects the author's research and analysis truthfully and completely.
- The paper properly credits the meaningful contributions of co-authors and co-researchers.
- The results are appropriately placed in the context of prior and existing research.
- All authors have been personally and actively involved in substantial work leading to the paper and will take public responsibility for its content.
- The authors have no competing interests.

CRediT authorship contribution statement

Iftikhar Ahmad: Formal analysis, Investigation, Methodology, Supervision, Validation, Visualization. **Syed Ibrar Hussain:** Conceptualization, Funding acquisition, Investigation, Methodology, Resources, Writing – original draft, Writing – review & editing. **Hira Ilyas:** Conceptualization, Data curation, Investigation, Software. **Muhammad Asif Zahoor Raja:** Investigation, Methodology, Resources, Supervision, Conceptualization, Formal analysis. **Sana Afzal:** Formal analysis, Investigation, Methodology, Software, Visualization, Writing – original draft. **Mariam Javed:** Data curation, Formal analysis, Investigation, Writing – review & editing.

Declaration of competing interest

The authors declare that they have no known competing financial interests or personal relationships that could have appeared to influence the work reported in this paper.

Data availability

Data will be made available on request.

References

[1] A.K. Awasthi, H. Kaur, A numerical study of transport of O2 and CO2 in a red blood cell, AIP Conf. Proc. 2768 (1) (2023, June) (AIP Publishing).
[2] I. Ahmad, H. Ilyas, S.I. Hussain, M.A.Z. Raja, Evolutionary techniques for the solution of bio-heat equation arising in human dermal region model, Arabian J. Sci. Eng. (2023) 1–26.
[3] A. Domínguez-Oliva, M.D. Ghezzi, P. Mora-Medina, I. Hernández-Ávalos, J. Jacome, A. Castellón, I. Falcón, F. Reséndiz, N. Romero, R. Ponce, D. Mota-Rojas, Anatomical, physiological, and behavioral mechanisms of thermoregulation in elephants, J. Anim. Behav. Biometeorol. 10 (4) (2022) 0-0.
[4] H.L. Dingwall, R.R. Tomizawa, A. Aharoni, P. Hu, Q. Qiu, B. Kokalari, S.M. Martinez, J.C. Donahue, D. Aldea, M. Mendoza, I.A. Glass, A transient dermal niche and dual epidermal programs underlie sweat gland development, bioRxiv (2023) 2023-04.
[5] M.A. Khanday, Numerical study of partial differential equations to estimate thermoregulation in human dermal regions for temperature dependent thermal conductivity, J. Egypt. Math. Soc. 22 (1) (2014) 152–155.
[6] A.U.H. Lone, M.A. Khanday, S. Mubarak, F.A. Reshi, Heat distribution and the condition of hypothermia in the multi-layered human head: a mathematical model, Comput. Methods Biomech. Biomed. Eng. 26 (1) (2023) 90–97.
[7] Z. Liu, J. Huang, D. Kang, Y. Zhou, L. Du, Q. Qu, J. Wang, L. Wen, D. Fu, Z. Hu, Y. Miao, Microenvironmental reprogramming of human dermal papilla cells for hair follicle tissue engineering, Acta Biomater. 165 (2023) 31–49.
[8] M. Singhal, R.K. Singla, K. Goyal, S. Singh, Inverse optimization based non-invasion technique for multiple tumor detection in brain tissue, Int. Commun. Heat Mass Tran. 141 (2023) 106596.
[9] S. Wang, F. Cheng, Q. Ji, M. Song, Z. Wu, Y. Zhang, Z. Ji, H. Feng, J.C.I. Belmonte, Q. Zhou, J. Qu, Hyperthermia differentially affects specific human stem cells and their differentiated derivatives, Protein & Cell 13 (8) (2022) 615–622.
[10] K. Cheng, B. Liu, X.S. Zhang, R.Y. Zhang, F. Zhang, G. Ashraf, G.Q. Fan, M.Y. Tian, X. Sun, J. Yuan, Y.D. Zhao, Biomimetic material degradation for synergistic enhanced therapy by regulating endogenous energy metabolism imaging under hypothermia, Nat. Commun. 13 (1) (2022) 4567.
[11] C. Bao, O. Chen, H. Sheng, J. Zhang, Y. Luo, B.W. Hayes, H. Liang, W. Liedtke, R.R. Ji, S.N. Abraham, A mast cell–thermoregulatory neuron circuit axis regulates hypothermia in anaphylaxis, Sci. Immunol. 8 (81) (2023) eadc9417.
[12] Y. Tokutake, R. Takanashi, M. Kikusato, M. Toyomizu, K. Sato, Effect of dietary 4-phenylbuthyric acid supplementation on acute heat-stress-induced hyperthermia in broiler chickens, Animals 12 (16) (2022) 2056.
[13] P.G. Firth, O.J. Benavidez, L. Fiechtner, The signs and symptoms of Ernest Shackleton, J. Med. Biogr. 31 (1) (2023) 10–15.

[14] E. Marshall, Appendix 6. Report on the health of the expedition, in: The Heart of the Antarctic, vol. 2, JB Lippincott Co, Philadelphia, 1909, pp. 426–428.
[15] F.C. Henriques, A.R. Moritz, Studies of thermal injury: I. The conduction of heat to and through skin and the temperatures attained therein. A theoretical and an experimental investigation, Am. J. Pathol. 23 (4) (1947) 530.
[16] H.H. Pennes, Analysis of tissue and arterial blood temperatures in the resting human forearm, J. Appl. Physiol. 1 (2) (1948) 93–122.
[17] H.L. Thron, Der Temperaturgradient in der menschlichen Gesichtshaut bei Einwirkung verschiedener Umgebungstemperaturen, Pflueg. Arch. Eur. J. Physiol. 263 (2) (1956) 109–126.
[18] W. Perl, Heat and matter distribution in body tissues and the determination of tissue blood flow by local clearance methods, J. Theor. Biol. 2 (3) (1962) 201–235.
[19] P.D. Richardson, J.H. Whitelaw, Transient heat transfer in human skin, J. Franklin Inst. 286 (3) (1968) 169–181.
[20] U. Flesch, The distribution of heat sources in the human head: a theoretical consideration, J. Theor. Biol. 54 (2) (1975) 285.
[21] A.M. Patterson, Measurements of temperature profiles in human-skin, South Afr. J. Sci. 72 (3) (1976) 78–79.
[22] V.P. Saxena, Application of similarity transformation to unsteady state heat migration problems in human skin and subcutaneous tissues, in: International Heat Transfer Conference, 6 Th, Toronto, Canada, 1978, pp. 65–68.
[23] V. Sxena, D. Arya, Variational finite element approach to heat distribution problems in human skin andSubdermal tissues, in: Proc. Ist Int. Conf. Numerical Methods in Thermal Problems, Pineridge Press, UK, 1979, pp. 1067–1076.
[24] V.P. Saxena, D. Arya, Steady-state heat distribution in epidermis, dermis and subdermal tissues, J. Theor. Biol. 89 (3) (1981) 423–432.
[25] D. Arya, Temperature distribution in human skin and subcutaneous tissues under radiation and evaporation conditions, Indian J. Pure Appl. Math. 14 (1983) 1398–1405.
[26] V. Saxena, BINDRA. JS steady state temperature distribution in dermal regions of human body with variable blood flow, perspiration and self-controlled metabolic heat generation, J, Pure Appl. Math. 15 (1) (1984) 31–42.
[27] K.R. Diller, L.J. Hayes, A finite element model of burn injury in blood-perfused skin, J. Biomech. Eng. 105 (3) (1983) 300–307.
[28] Y. Xuan, W. Roetzel, Bioheat equation of the human thermal system, Chem. Eng. Technol.: Ind. Chem.-Plant Equip.Process Eng. Biotechnol. 20 (4) (1997) 268–276.
[29] E.Y.K. Ng, L.T. Chua, Mesh-independent prediction of skin burns injury, J. Med. Eng. Technol. 24 (6) (2000) 255–261.
[30] M. Agrawal, N. Adlakha, K. Pardasani, Seminumerical model to study temperature distribution in peripheral layers of elliptical and tapered shaped human limbs, J. Mech. Med. Biol. 10 (1) (2010) 57–72.
[31] D.B. Gurung, V.P. Saxena, P.R. Adhikary, FEM approach to one dimensional unsteady state temperature distribution in human dermal parts with quadratic shape functions, J. Appl. Math. Inf. 27 (1_2) (2009) 301–313.
[32] S. Acharya, D.B. Gurung, V.P. Saxena, Time dependent temperature distribution model in layered human dermal part, Kathmandu Univ. J. Sci. Eng. Technol. 8 (2) (2012) 66–76.
[33] D.B. Gurung, Two dimensional temperature distribution model in human dermal region exposed at low ambient temperatures with air flow, Kathmandu Univ. J. Sci. Eng. Technol. 8 (2) (2013) 11–24.
[34] E. Kengne, A. Lakhssassi, R. Vaillancourt, Temperature distributions for regional hypothermia based on nonlinear bioheat equation of pennes type: dermis and subcutaneous tissues, Appl. Math. 3 (3) (2012) 217.
[35] I. Ahmad, S.I. Hussain, H. Ilyas, J.L. García Guirao, A. Ahmed, S. Rehmat, T. Saeed, Numerical solutions of Schrödinger wave equation and Transport equation through Sinc collocation method, Nonlinear Dynam. 105 (1) (2021) 691–705.
[36] I. Ahmad, S.I. Hussain, M. Usman, H. Ilyas, On the solution of Zabolotskaya–Khokhlov and Diffusion of Oxygen equations using a sinc collocation method, Part. Differ. Equ. Appl. Math. 4 (2021) 100066.
[37] I. Ahmad, H. Ilyas, K. Kutlu, V. Anam, S.I. Hussain, J.L.G. Guirao, Numerical computing approach for solving Hunter-Saxton equation arising in liquid crystal model through sinc collocation method, Heliyon 7 (7) (2021) e07600.
[38] I. Ahmad, S.U.I. Ahmad, K. Kutlu, H. Ilyas, S.I. Hussain, F. Rasool, On the dynamical behavior of nonlinear Fitzhugh–Nagumo and Bateman–Burger equations in quantum model using Sinc collocation scheme, Eur. Phys. J. Plus 136 (11) (2021) 1108.
[39] I. Ahmad, S.I. Hussain, M.A.Z. Raja, M. Shoaib, Qurratulain, Transportation of hybrid MoS 2–SiO 2/EG nanofluidic system toward radially stretched surface, Arabian J. Sci. Eng. 48 (1) (2023) 953–966.
[40] S.I. Hussain, I. Ahmad, M.A.Z. Raja, C.M.Z. Umer, A computational convection analysis of SiO2/water and MoS2-SiO2/water based fluidic system in inverted cone, Eng. Rep. 5 (11) (2023) e12660.
[41] I. Ahmad, S.I. Hussain, H. Ilyas, S. Jabeen, A. Iqrar, On the applications of collocation method for numerically analyzing the nonlinear Degasperis–Procesi and Benjamin–Bona–Mahony equations, Int. J. Mod. Phys. B (2023) 2450264.
[42] A. Sur, S. Mondal, M. Kanoria, Influence of moving heat source on skin tissue in the context of two-temperature memory-dependent heat transport law, J. Therm. Stresses 43 (1) (2020) 55–71.
[43] A. Sur, S. Mondal, M. Kanoria, Transient heating in a spherical tissue due to thermal therapy in the context of memory-dependent heat transport law, Waves Random Complex Media 32 (2) (2022) 887–905.
[44] A. Sur, Magneto-photo-thermoelastic interaction in a slim strip characterized by hereditary features with two relaxation times, Mech. Time-Dependent Mater. (2023) 1–26.
[45] S. Mondal, A. Sur, M. Kanoria, Healing of the cancer tissues under the action of moving heat and non-local Caputo–Fabrizio heat transport, Waves Random Complex Media 32 (6) (2022) 2606–2621.
[46] M. Marin, A. Hobiny, I. Abbas, The effects of fractional time derivatives in porothermoelastic materials using finite element method, Mathematics 9 (14) (2021) 1606.
[47] I. Abbas, A. Hobiny, M. Marin, Photo-thermal interactions in a semi-conductor material with cylindrical cavities and variable thermal conductivity, J. Taibah Univ. Sci. 14 (1) (2020) 1369–1376.
[48] F.S. Alzahrani, I.A. Abbas, Analytical estimations of temperature in a living tissue generated by laser irradiation using experimental data, J. Therm. Biol. 85 (2019) 102421.
[49] A. Alsisi, I. Abbas, K. Lotfy, A. El-Bary, M. Ahmed, The impact of fractional derivative on thermomechanical interactions in two-dimensional skin tissues throughout hyperthermia treatment, Case Stud. Therm. Eng. 54 (2024) 104025.
[50] A. Hobiny, I. Abbas, Analytical solutions of fractional bioheat model in a spherical tissue, Mech. Base. Des. Struct. Mach. 49 (3) (2021) 430–439.
[51] F.S. Alzahrani, I.A. Abbas, Analytical estimations of temperature in a living tissue generated by laser irradiation using experimental data, J. Therm. Biol. 85 (2019) 102421.
[52] M.A. Fahmy, Modeling and optimization of anisotropic viscoelastic porous structures using CQBEM and moving asymptotes algorithm, Arabian J. Sci. Eng. 44 (2) (2019) 1671–1684.
[53] M.A. Fahmy, A new LRBFCM-GBEM modeling algorithm for general solution of time fractional-order dual phase lag bioheat transfer problems in functionally graded tissues, Numer. Heat Tran., Part A: Applications 75 (9) (2019) 616–626.
[54] M.A. Fahmy, A computational model for nonlinear biomechanics problems of FGA biological soft tissues, Appl. Sci. 12 (14) (2022) 7174.
[55] M.A. Fahmy, Modeling and optimization of anisotropic viscoelastic porous structures using CQBEM and moving asymptotes algorithm, Arabian J. Sci. Eng. 44 (2) (2019) 1671–1684.
[56] H.C. Andrade, A.B.C.G. Silva, F.L.B. Ribeiro, L.C. Wrobel, A parallel implementation of a thermoregulation model using the finite element method, in: CILAMCE 2019: Proceedings of the XL Ibero-Latin-American Congress on Computional Methods in Engineering, 2019.
[57] A.S. Berahas, J. Shi, Z. Yi, B. Zhou, Accelerating stochastic sequential quadratic programming for equality constrained optimization using predictive variance reduction, Comput. Optim. Appl. (2023) 1–38.
[58] I. Ahmad, S.I. Hussain, H. Ilyas, L. Zoubir, M. Javed, M.A. Zahoor Raja, Integrated stochastic investigation of singularly perturbed delay differential equations for the neuronal variability model, Int. J. Intell. Syst. 2023 (2023).
[59] Z.I. Butt, I. Ahmad, M.A.Z. Raja, S.I. Hussain, M. Shoaib, H. Ilyas, Neuro-Heuristic computational intelligence approach for optimization of electro-magneto-

hydrodynamic influence on a nano viscous fluid flow, Int. J. Intell. Syst. 2023 (2023).
[60] Z.I. Butt, I. Ahmad, S.I. Hussain, M.A.Z. Raja, M. Shoaib, H. Ilyas, Inverse multiquadric kernel-based neuro heuristic approach to analyze the unsteady MHD nanofluid flow via permeable elongating surface, ZAMM-J. Appl. Math. Mech./Zeitschrift für Angewandte Mathematik und Mechanik 104 (2) (2024) e202300390.
[61] A. Kurani, P. Doshi, A. Vakharia, M. Shah, A comprehensive comparative study of artificial neural network (ANN) and support vector machines (SVM) on stock forecasting, Ann. Data Sci. 10 (1) (2023) 183–208.
[62] R.S. Kumar, I.G.C. Raj, I. Alhamrouni, S. Saravanan, N. Prabaharan, S. Ishwarya, M. Gokdag, M. Salem, A combined HT and ANN based early broken bar fault diagnosis approach for IFOC fed induction motor drive, Alex. Eng. J. 66 (2023) 15–30.
[63] Z.I. Butt, I. Ahmad, S.I. Hussain, M.A.Z. Raja, M. Shoaib, H. Ilyas, Intelligent computing paradigm for unsteady magneto nano-polymeric Casson nanofluid with Ohmic dissipation and thermal radiation, Chin. J. Phys. 88 (2024) 212–269.
[64] B. Zhao, P. Li, Y. Du, Y. Li, X. Rong, X. Zhang, H. Xin, Artificial neural network assisted bearing capacity and confining pressure prediction for rectangular concrete-filled steel tube (CFT), Alex. Eng. J. 74 (2023) 517–533.
[65] I. Ahmad, H. Qureshi, M.A.Z. Raja, S.I. Hussain, S. Fatima, A novel design of stochastic approximation treatment of longitudinal rectangular fin dynamical model, Case Stud. Therm. Eng. 54 (2024) 104042.
[66] M. Ehteram, A. Ferdowsi, M. Faramarzpour, A.M.S. Al-Janabi, N. Al-Ansari, N.D. Bokde, Z.M. Yaseen, Hybridization of artificial intelligence models with nature inspired optimization algorithms for lake water level prediction and uncertainty analysis, Alex. Eng. J. 60 (2) (2021) 2193–2208.
[67] S.I. Hussain, E. Toscano, An extensive investigation into the use of machine learning tools and deep neural networks for the recognition of skin cancer: challenges, future directions, and a comprehensive review, Symmetry 16 (3) (2024) 366.